Journal of Theoretical and Applied Information Technology
15th February 2026. Vol.104. No.3

ISSN: 1992-8645 www.jatit.org E-ISSN: 1817-3195

RHYTHM-GUIDED CONVOLUTIONAL NEURAL NETWORK SEGMENTAL TRANSITION ENTROPY-MODULATED LESION DISCRIMINATION COTTON LEAF DISEASE IDENTIFICATION

K. KARTHIGA[1], Dr. B. RAJDEEPA[2]

[1]Research Scholar, Department of Computer Science, PSG College of Arts & Science, Coimbatore, India
[2] Associate Professor and Head, Department of Information Technology, PSG College of Arts & Science, Coimbatore, India
E-mail: [1]karthigakanthanm@gmail.com, [2]rajdeepa@psgcas.ac.in

ABSTRACT

Cotton leaf disease presents significant diagnostic challenges due to inconsistent symptom expression, irregular lesion geometry, and background interference in open-field imagery. These issues reduce the reliability of conventional detection systems, which often struggle with symptom fragmentation, visual overlap, and class imbalance. To address these limitations, this research proposes a biologically inspired architecture titled CO-CNN (Caterpillar Optimization-Based Convolutional Neural Network). The model incorporates rhythm-guided adaptation, segmental coordination, and entropy-modulated parameter transitions to regulate convolutional behavior based on lesion-driven visual entropy. Unlike fixed-structure models, CO-CNN refines kernel scaling, dropout positioning, and gradient modulation in response to region-specific complexity, ensuring stability across asymmetric lesion patterns. The network performs segment-wise adjustment to retain lesion detail while suppressing irrelevant activations arising from field-induced noise. In evaluation, CO-CNN achieves 89.828% Overall Detection Efficiency and reduces Total Prediction Deviation to 10.172%, outperforming state-of-the-art models under identical test conditions. These results validate its ability to classify cotton leaf diseases with high sensitivity and precision, especially in real-world datasets where symptom boundaries are diffuse, visual distortions are common, and class distributions remain uneven.

Keywords: *CO-CNN, Cotton Leaf Disease, Entropy-Modulated Learning, Segmental Adaptation, Rhythm-Guided CNN, Lesion Discrimination*

1. INTRODUCTION

Cotton holds strategic importance in global agriculture, serving as a key raw material for textile production and supporting the livelihoods of millions of rural people. While its cultivation has benefited from improved seeds and farming techniques, cotton remains biologically vulnerable to various foliar diseases [1]. Infections such as Corynespora leaf spot, Xanthomonas leaf blight, Stemphylium leaf blight, and Myrothecium leaf necrosis commonly damage leaf structure, interfere with chlorophyll activity, and reduce boll development. These diseases often manifest as irregular spots, vein discoloration, and marginal necrosis, which can spread rapidly under humid and poorly drained conditions. Identifying these diseases in their early stages can be challenging, especially when symptoms resemble those of nutrient deficiencies or weather-related damage. Delayed diagnosis results in a reduced yield and lower fiber quality [2], [3]. Farmers relying solely on visual observation often miss early signs or misjudge the cause, highlighting the need for reliable disease recognition methods for uncontrolled field environments.

Detecting cotton leaf disease accurately presents complex challenges due to overlapping symptom patterns and irregular presentation. Similar discolorations may arise from different diseases, and some infections mimic environmental stress or insect injury [4], [5]. Early-stage lesions may appear faint or fragmented, often unnoticed until widespread damage occurs. The appearance of disease varies across leaf surfaces depending on age, angle, and sunlight exposure, making consistent diagnosis extremely difficult. Real-world imaging conditions compound the problem through variations in brightness, background clutter, or leaf curvature [6]. When multiple leaves overlap or twist, lesion visibility becomes obstructed, contributing to diagnostic gaps. In many instances, numerous infections coexist, introducing visually entangled lesions that demand precise discrimination across mixed symptom boundaries. This complexity calls for consistent observational methods that adapt to

real-world inconsistencies while maintaining lesion-specific accuracy [7].

Disease-specific recognition in uncontrolled environments requires a process that can prioritize lesion-specific visual signals while suppressing background distortions. Leaf-level textures, marginal degradations, and pigment disruptions must be interpreted precisely despite visual inconsistency [8]. Diseases such as Colletotrichum leaf blight or Macrophomina-induced wilting often introduce irregular patterns not confined to predictable regions, complicating uniform feature extraction [9]. Traditional observation methods often fail to identify such abnormalities when lesions blend into the natural background or display irregular boundaries. Field-level disease datasets collected under real-world conditions frequently exhibit noise, occlusion, and sharp intra-class variation, reducing the reliability of any standard fixed-parameter diagnostic approach [10]. Effective recognition systems must learn to distinguish between natural and pathological variation, even in mobile-captured samples, maintaining both speed and accuracy under varied operational conditions [11].

Nature offers scalable behavioural strategies that adapt efficiently to uncertain environments. Among them, caterpillars exhibit segment-wise navigation, flexible correction, and rhythmically synchronized progression traits that match the need for consistent learning in variable plant imagery [12]. These organisms balance exploration and coordination across their bodies to move through uneven foliage. Translating this principle into a model of behavior introduces mechanisms for segment-specific adjustment, parameter stability, and disturbance handling within the learning structure [13]. A system guided by this behavioural intelligence dynamically refines its internal control based on visual feedback from lesions. It does not rely on fixed thresholds or manual tuning but instead adapts to the disease complexity presented in each sample [14]. This adaptability ensures resilience in structured conditions and under mobile or resource-constrained deployment scenarios where real-time classification becomes essential. The harmony between segmental intelligence and lesion-focused precision supports scalable disease detection for real-world agricultural applications [15], [16].

1.1. Problem Statement

Recent literature on plant and cotton leaf disease identification demonstrates steady progress in convolutional and lightweight deep learning architectures, yet a persistent gap remains in handling symptom irregularity, lesion overlap, and entropy-driven visual uncertainty under real field conditions. Existing studies largely assume stable texture distribution, uniform lesion boundaries, or controlled imaging environments, which limits robustness in practical agricultural deployment. Reported models emphasize accuracy gains through architectural depth or transfer learning, though limited attention is given to adaptive internal regulation aligned with lesion complexity and spatial disorder. This gap motivates the present research, which responds directly to documented limitations by introducing a lesion-responsive, rhythm-guided learning framework capable of regulating convolutional behavior under mixed symptom visibility. The contribution is significant in positioning biological coordination principles as a structural solution to instability, class ambiguity, and background interference reported across recent cotton disease studies, thereby strengthening diagnostic reliability within uncontrolled agricultural environments.

Identifying cotton leaf diseases under natural field conditions remains a critical and unresolved challenge. Disease symptoms often present as irregular blotches, discolorations, or marginal necrosis closely resembling environmental stressors or nutritional imbalances. The visual overlap between different disease types, inconsistent lesion distribution, and fragmented leaf surface exposure leads to frequent misclassification. External factors, such as poor lighting, background noise, overlapping foliage, and non-uniform image angles, further compromise visual clarity. Real-world cotton leaf datasets often suffer from class imbalance, variable image quality, and mixed infection patterns, where multiple diseases manifest on a single leaf. Early-stage signs are subtle and easily overlooked, while later-stage symptoms may already signal irreversible damage. Manual inspection is labor-intensive, inconsistent among observers, and often fails to provide timely, disease-specific insights. These constraints severely affect intervention timing, delay treatment measures, and ultimately contribute to yield reduction and the production of poor-quality fiber.

1.2. Motivation

Sustaining high-yield cotton cultivation depends on the early identification and targeted control of leaf diseases before irreversible damage occurs. Even minor delays in diagnosis can compromise photosynthetic efficiency, reduce boll

formation, and result in economic losses. With changing climate conditions and intensified monoculture practices, cotton crops face increasing exposure to rapidly spreading foliar infections. Most farmers operate without structured diagnostic support or access to expert agronomists, instead relying on subjective field observations. Reliable and consistent early-stage disease recognition becomes paramount in such contexts. The broader agricultural ecosystem, including researchers, agri-tech developers, and crop advisors, also requires tools to deliver standardized, scalable, and precise diagnostic outcomes across diverse field scenarios. This research is driven by the goal of supporting healthy cotton production cycles where disease identification is fast, robust, and sensitive to both visual complexity and operational constraints, enabling more resilient and profitable cultivation practices.

1.3. Objective

The objective of this research is to develop and implement a novel model, titled CO-CNN (Caterpillar Optimization-Based Convolutional Neural Network), to address the persistent limitations in cotton leaf disease detection under uncontrolled environmental conditions. The proposed work addresses key challenges, including mixed symptom visibility, high intra-class variation, lesion background confusion, and training instability. CO-CNN introduces an adaptive framework inspired by the segment-wise movement intelligence of caterpillars, allowing for dynamic tuning of dropout rates, kernel sizes, batch normalization, and gradient flow based on lesion-specific complexity. The model ensures robust classification across varying imaging conditions by integrating segmental coordination, entropy-driven diversity maintenance, and real-time convergence acceleration. The architecture is optimized for diagnostic accuracy and computational efficiency, making it suitable for resource-constrained and mobile deployments. This work proposes a scalable, lesion-aware, and context-sensitive disease identification system tailored to practical cotton farming environments.

The research design was selected to align explicitly with the objective of achieving stable cotton leaf disease identification under uncontrolled field conditions characterized by lesion irregularity, background interference, and class overlap. A biologically inspired adaptive convolutional framework was adopted since fixed-parameter or static deep learning designs reported in recent literature show reduced robustness under such variability. The design integrates lesion-driven entropy analysis, segment-wise parameter coordination, and adaptive regulation of kernels, dropout, normalization, and gradient flow, enabling direct operationalization of the stated objectives within the model structure itself. Each design component corresponds to a specific challenge identified in the problem formulation, ensuring methodological coherence rather than generic model selection. Suitability is demonstrated through evaluation metrics that reflect reliability, balance, deviation control, and lesion-focused precision, confirming that the chosen design provides a direct and measurable pathway for addressing the research questions.

1.4. Organization of the Paper

The Introduction explains the inconsistencies in cotton leaf image quality and the need for adaptable recognition mechanisms. The Literature Review outlines general advancements in leaf disease prediction methods using convolutional learning systems under field conditions. The Methodology introduces Caterpillar Optimization-Based Convolutional Neural Network, where caterpillar locomotion inspires dynamic segment-based tuning across layers, dropout, kernel shapes, and gradient propagation. The Dataset and Performance Metrics section describes the diversity of symptoms captured, the conditions under which images were acquired, and the quantitative performance indicators. The Results and Discussion section highlights how CO-CNN handles lesion noise, maintains feature clarity, and stabilizes learning across class variations. The Conclusion concludes with remarks on operational flexibility and real-time readiness for cotton disease classification.

2. LITERATURE REVIEW

The literature used to justify the research problem was selected through a structured relevance-based screening to ensure representativeness, recency, and technical adequacy. Emphasis was placed on recent peer-reviewed studies addressing plant and cotton leaf disease identification using deep learning under real or semi-uncontrolled conditions. Works were chosen to reflect diverse methodological trends, including transfer learning, lightweight convolutional models, attention-based architectures, optimization-driven learning, and multimodal diagnostic systems. Studies limited to controlled environments or static feature assumptions were excluded. Adequacy was ensured by prioritizing publications that explicitly report challenges related to lesion irregularity, class imbalance, background interference, or symptom

overlap. Cross-validation of reported limitations across multiple sources was used to confirm consistency, ensuring the reviewed literature provides a current and representative foundation for problem justification.

The "Multimodal Fusion Framework (MFF)" [101] provides a cooperative mechanism that integrates leaf imagery and environmental time logs. The CNN observes fixed visual attributes from leaf surfaces, identifying deformities or lesions. The RNN concurrently reads climate sequences, such as temperature shifts, and detects triggers that promote disease spread. Both predictions are merged using confidence-weighted integration, aligning spatial detail with real-time environmental influences. This structure helps mitigate single-view blind spots by encouraging cross-validation across modalities. The system adapts well to unexpected weather patterns or rare disease expressions, offering actionable insights for disease management. Its architecture promotes resilience and modularity in diverse field settings. "SmartCotton TL-Scan (SCTLS)" [17] presents a framework for identifying cotton leaf diseases using optimized transfer learning and web deployment. Multiple pre-trained CNNs are tested and fine-tuned, with Xception demonstrating superior performance. Parameters are tuned layer by layer to improve lesion detection. The model is integrated into a browser-based application, enabling farmers to upload leaf images and receive instant disease classifications. Image processing occurs in real-time, supporting inference under limited connectivity. Feature scoring adds transparency to predictions. Model reliability and low computational load enable accessible and accurate disease diagnosis in rural settings. The system design allows extensions for diagnosing diseases in other crop domains.

"TomatoLite IRCA-Net" [18] presents a compact model for tomato disease detection based on MobileNetv3, which integrates inverted residual units and channel attention. Depthwise separable convolutions efficiently extract leaf features, while residual blocks expand and compress channels to capture subtle disease cues. Channel attention gates highlight disease-relevant features, suppressing healthy background noise. Hard-swish activation boosts shallow layer discrimination. The efficient design maintains accuracy under varied conditions and is suitable for mobile use, supporting scalable detection for tomato growers. "GrapeYOLO-ACCW" [19] adapts YOLOv8 for lightweight grape disease detection, introducing the Adaptive Convolution-Coupled Window (ACCW) module for small lesions and spatial ambiguity handling. Region-specific attention adapts receptive fields, and residual refinement stabilizes training. Optimized feature pyramids and bounding box center-weighting enhance precision. Focal loss reduces false positives, and group convolutions compress the model for mobile deployment. GrapeYOLO-ACCW enables real-time vineyard disease identification under power and memory constraints. "PalmCare Hybrid System" [20] combines sensor diagnostics and deep learning for palm leaf disease monitoring. Visual leaf imagery and sensor data (temperature, chlorophyll, moisture) are fused via a CNN with attention and morphological filters. Sensor data is normalized and merged at the decision layer. A rule-based module prescribes agrochemical dosages or alerts, adapting treatment logic based on the feedback received. Therapy optimization and scheduling are informed by recorded outcomes, enabling adaptive, real-time palliative care with integrated sensing and vision. "FedTransform WheatScan" [21] uses transformer vision models and federated learning for privacy-preserving wheat disease detection. Each client trains a local transformer on wheat images, focusing on spatial lesion dependencies. Encrypted weight updates are aggregated centrally. Positional encoding and transfer layers enhance robustness to lighting and regional variations. Memory-augmented training manages disease progression snapshots. The distributed setup unifies knowledge across farms, outputting class predictions and interpretable attention maps while preserving data privacy.

"MangoX ExplainNet" [22] offers a feature-transparent convolutional model for mango disease diagnosis, using X-shaped residual units and depthwise convolutions. Multi-layer attention gates refine filters for fungal spread and color transitions. Adaptive preprocessing enhances lesion visibility. The model outputs class decisions and heatmaps, visualizing prediction cues and ranking the influence of diseases. Its explainability module maps lesion confidence, balancing interpretability and performance through modular design and filter redundancy reduction. "RAI-TomatoVision" [23] merges residual connections, inception modules, and spatial attention for tomato disease recognition. Residual links stabilize gradients, inception blocks capture varied patterns, and attention units focus on infected segments. Features are fused for nuanced encoding and the suppression of false cues. Cross-entropy loss and auxiliary branches guide learning and attention supervision. The final classifier outputs disease types, and attention maps allow inspection of feature dominance in predictions. "T-YOLO UAV-

RiceNet" [24] enhances rice disease detection for UAVs using a streamlined YOLOv4-Tiny variant. Redesigned feature pyramids and anchor-free decoding support multi-scale lesion recognition in aerial images. Dilated convolutions expand receptive fields, and contextual encoding manages prediction noise. GPS and altitude metadata filter environmental artifacts. Detections are tracked over UAV paths, ensuring consistent lesion tagging. The lightweight model fits embedded GPUs, enabling onboard, real-time inference. "MoS_2 Wetness Probe" [25] studies MoS_2 nanoflower-coated flexible sensors for quantifying leaf wetness. Nanoflowers increase sensitivity to microfilm moisture, with impedance changes signaling wetness. Sensors on polyimide substrates are tested for dynamic range, linearity, and durability under bending and temperature fluctuations. Impedance spectroscopy tracks moisture cycles, enabling accurate in-field estimation of leaf wetness duration for crop health diagnostics.

"Curvature-Aware Wetness Sensor" [26] evaluates flexible wetness sensors on curved leaf surfaces. Sensors on polyimide substrates measure the electrical response under controlled bending, simulating the natural movement of leaves. Signal drift, capacitive mismatch, and moisture retention are analyzed across curvatures. Finite element analysis maps strain, and compensation models recalibrate sensor response. Combined datasets inform a regression model for identifying optimal performance zones, thereby improving the real-world adaptability of leaf wetness sensing. "Cascade-Attention U-NetLeaf" [27] introduces a dual-stage framework for plant disease recognition. An attention-infused residual U-Net segments lesions, retaining boundary detail and suppressing irrelevant regions. A stacked autoencoder compresses lesion features, which are classified by a lightweight head. Cascading ensures semantic continuity, prioritizing lesion-centric features. Outputs include multi-class labels and visual masks, streamlining pixel-wise segmentation and label generation within a single pipeline. "LeafVision Bibliometric Map" [28] builds a bibliometric framework to analyze deep learning trends in plant disease detection. Citation data forms co-authorship and keyword networks, revealing core topics and research schools. Trend plots show the evolution of methods, and geographical heatmaps track research output. Journal overlays and conceptual timelines illustrate shifts from handcrafted features to hybrid models. Institutional and funding linkages are mapped, providing a dashboard for research hotspots and integration opportunities. "MaizeNet CropGuard" [29] presents a CNN for maize disease identification using hierarchical modules and refinement layers. Images are preprocessed for contrast and variance. Early layers extract lesion patterns; mid-level filters encode spot density. Channel-wise dropout regularizes training, and global max pooling abstracts features. A softmax classifier distinguishes disease types, with attention heatmaps highlighting key regions. The architecture is scalable and adaptable to other crops via feature layer fine-tuning.

Bio-inspired optimization in this work is adopted as a principled mechanism to regulate learning behavior under visual uncertainty rather than as a metaphorical enhancement [30]-[37]. The optimization strategy draws from segmented biological coordination, where adaptive response emerges through localized adjustment and inter-segment interaction [38]-[47]. This principle is mapped to convolutional learning by enabling controlled adaptation of kernels, dropout, normalization, and gradient flow in response to lesion complexity and entropy variation. The optimization process emphasizes stability, balance, and responsiveness within irregular visual environments, aligning model behavior with the non-uniform nature of cotton leaf disease patterns [48]-[60]. By embedding adaptive control directly into parameter transitions, the optimization framework supports consistent convergence and robust discrimination without reliance on rigid configurations or exhaustive manual tuning.

3. CATERPILLAR OPTIMIZATION-BASED CONVOLUTIONAL NEURAL NETWORK

To ensure that research findings are not influenced by unnecessary variation, multiple methodological control mechanisms were applied throughout model design, training, and evaluation. Input images were standardized through uniform resizing, normalization, and consistent preprocessing to reduce illumination and scale variability. All comparative models were trained and tested using identical datasets, class distributions, and evaluation protocols to maintain experimental fairness. Parameter instability was controlled through entropy-regulated learning rates, lesion-aware dropout adjustment, and batch normalization scaling guided by activation statistics. Randomness introduced during training was limited through fixed initialization ranges and controlled perturbation bounds. Performance assessment relied on multiple complementary metrics rather than a single accuracy measure, reducing metric bias. These controls

collectively isolate the effect of the proposed framework and ensure that observed performance differences arise from methodological design rather than uncontrolled experimental fluctuations.

Caterpillar Optimization-based Convolutional Neural Network (CO-CNN) is specifically proposed to address the variability and ambiguity in cotton leaf disease images. Unlike conventional models that apply uniform learning behaviours across all samples, CO-CNN introduces a synchronized optimization structure that adjusts layer responses based on lesion-specific complexity, entropy patterns, and spatial symptom inconsistency. The model integrates a rhythmically coordinated learning process inspired by segmented biological movement, allowing local feature adjustments to influence global stability without disrupting the overall learning path. Each phase of the framework is designed to function in alignment with symptom progression, ensuring adaptability under uncontrolled visual conditions. CO-CNN avoids rigid configuration and instead promotes coordinated responsiveness across parameters such as dropout, kernel dimensions, and gradient flow. The following steps outlined in the methodology reflect this principle, emphasising lesion-guided parameter control and adaptive convergence aligned with the real-world conditions of cotton cultivation.

3.1. Hyperparameter Optimization for Disease-Specific CNN Training

The segmented locomotion of a caterpillar signifies ordered coordination among multiple body segments, guiding movement through synchronous contractions and extensions. Mimicking this behavior in Convolutional Neural Networks (CNNs), the Caterpillar Optimization (CO) strategy initiates segmented hyperparameter encoding across kernel sizes, batch sizes, learning rates, and dropout probabilities. These elements collectively influence disease detection outcomes and model reliability in image-based classification tasks, particularly when dealing with cotton leaf disease patterns that exhibit variations in lesion texture, color distortion, and shape irregularity. Let ϕ_i represent the parameter segment corresponding to the i-th hyperparameter in the model. The collective parameter vector Φ at iteration t is given by:

$$\Phi^{(t)} = \left[\phi_1^{(t)}, \phi_2^{(t)}, \phi_3^{(t)}, \ldots, \phi_d^{(t)}\right] \quad (1)$$

Where, d indicates the number of hyperparameter segments considered for optimization. Each $\phi_i^{(t)}$ evolves through biologically inspired contraction-extension coordination, with dynamic fitness driving their movement toward parameter zones that yield efficient classification over cotton leaf datasets.

Each segment ϕ_i is evaluated in the context of input variability in diseased and non-diseased cotton leaves. A density-aware mechanism tunes the movement magnitude δ_i, controlling its direction based on spatial lesion variability embedded within the training data. Parameter ϕ_i evolves based on the weighted change defined by:

$$\delta_i^{(t)} = \gamma \cdot \left(\eta_i^{(t)} - \lambda_i^{(t)}\right) \quad (2)$$

Where, coefficient γ represents the caterpillar's segment movement sensitivity. Variable $\eta_i^{(t)}$ captures the current local update potential, while $\lambda_i^{(t)}$denotes the prior segment's resistance to change. This relational evolution pattern reduces arbitrary shifts in kernel scale or dropout values, especially when classifying early-stage infections.

Cotton leaf disease images present lesion features with a high intra-class variation. The segmentation-inspired reinforcement in CO ensures dynamic parameter influence across multiple epochs. Each parameter segment updates not in isolation, but relative to adjacent behavior, ensuring that lesion features at more minor scales are not suppressed during feature map propagation. Let the reinforcement coefficient matrix $R \in R^{d \times d}$ guide mutual influence among hyperparameters. The reinforcement update for each parameter is given by:

$$\phi_i^{(t+1)} = \phi_i^{(t)} + \sum_{j=1}^{d} R_{ij} \cdot \delta_j^{(t)} \quad (3)$$

The scalar R_{ij} captures the relationship between segments $i$and j, reflecting inter-parameter coordination such as kernel-dropout coupling or learning rate-batch size dependency. By reinforcing based on surrounding parameters, convergence toward effective disease classification is biologically stable and data-driven. To maintain relevance to real lesion presentation, R_{ij} is not static but periodically refreshed based on internal feedback from segmentation-driven class activation maps. This matrix-oriented refinement improves decision boundaries among disease categories with subtle visual overlaps.

Following the caterpillar's movement waveform across its segments, parameter adjustment in CO exhibits oscillatory behavior. Instead of linear tuning, the update paths are adjusted with context-

dependent acceleration or deceleration, modeled on the progression of cotton disease complexity. An epoch-based modulation function is introduced as:

$$\phi_i^{(t+1)} = \phi_i^{(t)} + sin(\omega_t) \cdot \delta_i^{(t)} \quad (4)$$

The sinusoidal term $sin(\omega_t)$ introduces a non-uniform modulation into the update pattern. The variable ω_t represents the phase adjustment determined by epoch count and classification entropy. When entropy is high, more aggressive exploration occurs; during stabilization, minor oscillations facilitate the exploitation of refined disease-discriminating regions. This progression stabilizes model generalization, especially in complex background images of diseased cotton leaves. Oscillatory segment adaptation minimizes overshooting in learning rate or over-pruning through dropout during early and middle training phases.

Caterpillars adapt their segment reach based on obstacle detection through sensory inputs. Mimicking this, the visual complexity of cotton leaf lesions influences the stretch of each parameter's allowable range. A region-aware expansion index ζ_i modulates parameter scope adaptively. The hyperparameter range for each segment is given by:

$$\phi_i^{(t)} \in \left[\phi_{min,i} + \zeta_i^{(t)}, \phi_{max,i} - \zeta_i^{(t)}\right] \quad (5)$$

The index $\zeta_i^{(t)} = \alpha \cdot C_i^{(t)}$, where $C_i^{(t)}$ represents the visual complexity index of cotton disease images associated with segment i. Coefficient α adjusts stretch flexibility. Larger lesion complexity leads to tighter bounds for learning rate and dropout; simpler structures expand the freedom of exploration. This contextual contraction and expansion of parameter zones ensure that the CNN configuration does not oversimplify or overfit to visually dominant disease classes. The goal remains robust classification of overall disease types and conditions.

To preserve diversity in parameter tuning across segments, a coupling mechanism influenced by inter-segmental tension, like that observed in caterpillar crawling, is incorporated. The elastic coupling introduces resistance or support depending on the diversity among segment directions. The update equation for coupled segments is expressed as:

$$\phi_i^{(t+1)} = \phi_i^{(t)} + \rho \cdot \sum_{j \neq i} k_{ij}^{(t)} \cdot \left(\phi_j^{(t)} - \phi_i^{(t)}\right) \quad (6)$$

Where, $k_{ij}^{(t)}$ represents the diversity weight between segments $i$and j, while ρ governs coupling elasticity. High k_{ij} implies significant parameter divergence, triggering elastic retraction or expansion, depending on direction. This strategy avoids convergence into parameter regions biased toward any singular disease pattern, promoting multi-class sensitivity.

Through this dynamic, CO-CNN adapts hyperparameter progression across disease types without losing directional learning fidelity. Elastic coupling increases sensitivity to inter-class boundary refinements.

3.2. Progressive Learning Rate Scheduling

In biological locomotion, the caterpillar progresses through rhythmic contractions and extensions across its body segments, adjusting the intensity of these movements based on the complexity of the terrain. Emulating this principle, the progressive learning rate scheduling strategy initiates epoch-sensitive adjustments that mimic contraction-relaxation dynamics for stable CNN training in cotton leaf disease classification. The scheduling adapts to both the visual complexity of leaf images and the learning saturation level of the model during training cycles. Let the base learning rate at epoch e be denoted by λ_e, modulated rhythmically using a sigmoid compression around epoch intensity:

$$\lambda_e = \lambda_0 \cdot \frac{1}{1 + exp\left(\mu_e \cdot (e - \theta)\right)} \quad (7)$$

Where, λ_0 is the initial learning rate, μ_e represents the sigmoid sharpness controlling responsiveness, e is the epoch number, and θ is the saturation threshold when feature abstraction nears convergence. As training progresses, the learning rate compresses based on the intensity shift μ_e, reducing the risk of overshooting minima during fine-tuning stages.

This rhythmically diminishing pattern is tuned to adjust the model's step size when cotton leaf lesions become harder to differentiate in deeper CNN layers, especially during minor texture variations across disease types. As caterpillars reduce movement speed upon sensing unstable terrain, learning rate dampening serves as a corrective mechanism to avoid training oscillations. The adaptive variance-based modulation model stabilizes updates when classification confidence fluctuates, particularly in the presence of ambiguous disease regions. The dampened learning rate $\tilde{\lambda}_e$ is given by:

$$\tilde{\lambda}_e = \lambda_e \cdot \left(1 - \frac{\sigma_\epsilon^2}{\sigma_{max}^2 + \epsilon}\right) \quad (8)$$

Where, σ_ϵ^2 represents the prediction variance across mini-batches at epoch e, σ_{max}^2 is the global maximum variance observed, and ε is a smoothing

constant. This ensures the learning rate scales down when instability peaks during lesion misclassification. Reduced learning steps mitigate divergence risks and align CNN updates with terrain-like resistance modeled from biological foraging response.

Training in CNNs often exhibits curvature-dependent learning dynamics where sharp curvature regions demand smaller step sizes. The learning rate curvature coupling introduces attenuation by mapping activation gradient sensitivity from classification loss surfaces. Let k_e denote the local curvature estimated via second-order gradients, leading to:

$$\lambda'_e = \tilde{\lambda}_e \cdot exp(-\gamma \cdot k_e) \quad (9)$$

The coefficient γ modulates exponential decay sensitivity to curvature k_e, which represents the steepness of the error surface for disease classification regions. Sharper curvatures reduce the effective learning rate, minimizing the risk of parameter oscillation, especially near high-impact misclassified leaf patches. This approach mirrors the caterpillar's adaptive slowing response in sharply inclined terrain, embedding visual difficulty sensitivity into the learning schedule.

Cotton leaf images may possess regions with highly irregular visual entropy, especially when disease boundaries are blurred. The optimizer must expand exploration velocity in these zones to capture subtle lesion patterns. Visual entropy H_e is mapped using information content from feature activations:

$$\lambda''_e = \lambda'_e + \delta \cdot \frac{H_e}{H_{norm}} \quad (10)$$

The variable δ indicates a scalar velocity enhancer, H_e is the entropy derived from CNN intermediate activations, and H_{norm} is the normalization constant. When entropy is high, the learning rate is temporarily increased to enable the model to explore alternative solutions, much like a caterpillar stretching its segments to navigate uncertain surfaces.

Inspired by how caterpillars propagate mechanical tension across adjacent segments, temporal elasticity is introduced across training epochs. Segmental propagation coefficients β_i enable inter-epoch learning rate inheritance based on prior success in disease-specific classification. The temporally elastic learning rate is computed as:

$$\lambda^*_e = \lambda''_e + \sum_{i=1}^{n} \beta_i \cdot sin(\xi_e \cdot i) \quad (11)$$

Where, $\beta_i$encodes the influence of the i-th CNN layer on learning rhythm, and ξ_e adjusts propagation amplitude across epochs. This formula mimics real-time feedback in caterpillar movement, where segment strain at one end influences the flexibility of another. By applying sinusoidal perturbations, this temporal inheritance sharpens convergence over similar lesion types across different epochs.

Some cotton disease images display localized regions with near-zero classification confidence. During such regions, learning must be suppressed to avoid noise amplification. Let U_r represent the regional uncertainty score computed via entropy margin difference:

$$\lambda^\dagger_e = \lambda^*_e \cdot (1 - \zeta \cdot U_r) \quad (12)$$

Where, ζ represents the uncertainty suppression coefficient. The scalar U_r reflects intra-class ambiguity in the activated lesion region, derived from drops in feature map entropy. Suppressing the learning rate during such regions enables smoother feature discrimination development and reduces training instability associated with noisy lesion patterns.

Cotton leaf lesions often shift position across image samples, requiring localized feedback-driven rate correction. A reinforcement loop captures lesion attention deviation to adjust learning rates around high-impact pixels. Define lesion-centric correction weight α_e as:

$$\lambda^{\neq}_e = \lambda^\dagger_e + \eta \cdot \left(\frac{\Delta A_e}{A_e + \epsilon}\right) \quad (13)$$

Here, Variable η regulates lesion deviation impact, ΔA_e is the attention shift from the previous to the current epoch, and A_e is the baseline attention magnitude. Reinforcement scaling allows the optimizer to recover missed lesion zones and refine focus for better disease boundary detection in complex classification regions.

3.3. Disease-Driven Regularization via Adaptive Dropout

Caterpillar locomotion adapts dynamically to terrain variations by precisely controlling leg support distribution. Similarly, dropout regularization in CNNs must align with the spatial and statistical density of lesions observed in cotton leaf disease datasets. Adaptive dropout in this context refers to dynamically altering the dropout probability based on local lesion information embedded in the convolutional feature maps. Let the dropout probability for a given neuron group at training iteration t be denoted as $p^{(t)}$. The initial

dropout probability is refined through a lesion-density-sensitive adjustment mechanism given by:

$$p^{(t)} = \rho \cdot \left(1 + \frac{L_d^{(t)}}{L_{max} + \epsilon}\right) \quad (14)$$

Where, ρ indicates the baseline dropout upper limit, $L_d^{(t)}$ represents the current average lesion density across a mini-batch, L_{max} is the maximum observed lesion density, and ϵ is a non-zero stabilizer. As lesion concentration increases, the dropout rate is adaptively reduced, ensuring higher retention of discriminative neurons. This reflects how caterpillars minimize leg lifting in denser terrain zones to maintain grip.

Cotton leaf diseases present wide inter-class visual differences in lesion patterns. To capture class-specific neuron retention, the dropout probability is refined using a divergence score D_c across disease types, embedded in the following relation:

$$p_c^{(t)} = p^{(t)} \cdot \left(1 - \delta \cdot \frac{D_c}{D_{ref} + \epsilon}\right) \quad (15)$$

Where, D_c refers to the divergence score of the current disease class from a reference class baseline D_{ref}, and δ adjusts the modulation strength. High divergence indicates that a class requires more stable neuron pathways to prevent the loss of unique features, thereby reducing dropout further. This parameter tuning replicates how caterpillar segments react differently when navigating visually dissimilar terrain regions.

The dropout rate must be adjusted not only spatially but also temporally across epochs. Drawing on the caterpillar's tendency to distribute movement energy differently at early and later stages of navigation, the temporal dropout attenuation mechanism defines the adjusted probability as:

$$p_e^{(t)} = p_c^{(t)} \cdot \left(\frac{1}{1 + \omega \cdot e}\right) \quad (16)$$

Where, ω represents the epoch influence coefficient and e denotes the current training epoch. As training advances, dropout is reduced to consolidate learned patterns. This strategy mirrors the caterpillar's decreasing lift behavior as it moves into stable terrain segments, promoting more continuous contact.

Dropout regularization can be further enhanced by targeting the suppression of neurons that exhibit high activation variability over epochs. A neuron's instability score $\chi_i$is used to define the refined dropout rate p_i per neuron as:

$$p_i = p_e^{(t)} + \eta \cdot \frac{\chi_i}{\chi_{max} + \epsilon} \quad (17)$$

Where, η is the sensitivity scalar for variability influence, χ_i denotes the temporal activation variance of neuron i, and χ_{max} is the highest recorded variance. Neurons with erratic behavior are dropped more frequently, resembling how caterpillars disengage weaker or unstable body segments when progressing forward on unreliable terrain.

A lesion attention map generated from intermediate CNN layers enhances the granularity of spatial dropout. Let $A_{x,y}$ denote the attention score at the spatial coordinate (x, y).The spatial dropout mask $M_{x,y}$ is generated using a probability thresholding scheme:

$$M_{x,y} = \begin{cases} 0, & if\ A_{x,y} < \tau \\ 1, & otherwise \end{cases} \quad (18)$$

The threshold τ is dynamically computed based on lesion sharpness gradient statistics, enabling neurons associated with less relevant spatial patches to be suppressed. The dropout mask resembles the caterpillar's ability to disengage support from less essential limb segments while emphasizing the regions that provide the most secure grip.

Elastic segment coordination observed in caterpillar movement motivates the redistribution of dropout probability across layers based on structural strain. The dropout redistribution vector $\vec{p}l$ for layer l is governed by:

$$\vec{p}l = p_e^{(t)} \cdot \left(1 + \sigma_1 \cdot cos(\theta_l)\right) \quad (19)$$

Where, σ_1 represents the strain coefficient extracted from weight update magnitudes, and θ_l is the angular shift derived from filter orientation changes in layer l. Layers experiencing mechanical strain—analogous to caterpillar body segments adjusting angle and length—undergo moderated dropout, enhancing feature stability and directional learning.

Disease subclasses may exist under broader class categories, requiring fine-grained neuron discrimination. A subclass attention weight α_s scales the dropout probability, producing a subclass-adjusted dropout rate:

$$p_s^{(t)} = p_e^{(t)} \cdot \left(1 - \alpha_s \cdot log(1 + \zeta_s)\right) \quad (20)$$

Where, ζ_s indicates subclass entropy, representing classification ambiguity within a class. Lower entropy signifies clear visual patterns, enabling slightly higher dropout, while higher entropy lowers dropout to preserve neurons responsible for subtle subclass distinctions. The scaling ensures better retention of subclass boundaries, reflecting how

caterpillars reduce leg disengagement under highly fragmented terrain.

The dropout scheduling process adheres closely to the caterpillar's strategy of minimizing risk through adaptive support withdrawal, ensuring that CNNs maintain balanced learning capacity across cotton disease classes without excessive neuron loss. Each dropout strategy embeds visual lesion awareness and structural stability into the training process.

3.4. Multi-Scale Kernel Selection for Disease Variability

Caterpillar locomotion adjusts the span of body segments depending on environmental texture and obstacle size. Translating this biological principle to Convolutional Neural Networks (CNNs), kernel scope must be flexibly tuned across layers to adapt to variations in lesion scale and structure in cotton leaf disease samples. Kernels must not remain static, as lesion boundaries differ in thickness, shape, and distribution. The adaptive kernel selection function k_s for scale s is defined by:

$$k_s = \lambda_k \cdot \left(1 + \frac{\xi_s}{\xi_{ref} + \epsilon}\right) \quad (21)$$

Where, λ_k represents the base kernel size. The variable $\xi_s$captures lesion contour sharpness in the current scale, and ξ_{ref} provides a global reference to ensure bounded scaling. A sharper lesion results in broader receptive fields, promoting better spatial coverage for disease identification.

Lesion spread in cotton leaves varies across disease types. To ensure proportional spatial filtering, a convolutional coverage index C_l is used to refine kernel placement across layers:

$$C_l = \frac{1}{Z_l} \sum_{i=1}^{h_l} \sum_{j=1}^{w_l} \left(\frac{\psi_{ij}}{\psi_{max} + \epsilon}\right) \quad (22)$$

Where, ψ_{ij} denotes the lesion pixel intensity at location (i, j), $h_l$and w_l are height and width of the activation map in layer l, $Z_l = h_l \cdot w_l$, and ψ_{max} is the highest lesion intensity recorded. The resulting C_l determines the proportion of lesion-occupied regions. Larger C_l values result in wider kernels, mimicking segment extension in terrain-dense zones during caterpillar progression.

Cotton leaf lesions often present asymmetrical boundaries. To accommodate this, the aspect ratio α_r of kernels is tuned using boundary elongation metrics derived from horizontal and vertical lesion components:

$$\alpha_r = \frac{E_h}{E_v + \epsilon} \quad (23)$$

Where E_h and E_v represent elongation values along horizontal and vertical directions respectively, calculated using the lesion shape's principal axis projections. Kernels are reshaped dynamically to align with dominant lesion orientation, reflecting caterpillar body orientation shifts in response to narrow or elongated pathways.

At deeper CNN layers, the lesion abstraction becomes increasingly complex. To retain sensitivity, hierarchical kernel scale selection is guided by activation entropy H_l:

$$H_l = -\sum_{i=1}^{n_l} p_i . log(p_i + \epsilon) \quad (24)$$

Where p_i indicates the normalized activation value at neuron i in layer l, and n_l represents the total neurons in the layer. Higher entropy reflects spatial inconsistency in lesion abstraction, prompting dynamic expansion of kernel size in that layer. This emulates segment elongation under uncertain terrain feedback in caterpillar locomotion.

Disease-specific textures often overlap in feature space. A multi-path kernel setup is introduced where different kernel sizes $k_1, k_2, \ldots, k_n$ operate in parallel and are fused through weighted summation:

$$O = \sum_{s=1}^{n} \omega_s \cdot \phi_s(x) \quad (25)$$

Where, ω_s denotes the adaptive weight for scale s, and $\phi_s(x)$ represents the feature map generated by kernel of size k_s applied to input x. The weight ω_s is derived from texture separation statistics, enabling distinct processing of different lesion types. The fusion mechanism replicates how caterpillars utilize multiple micro-adjustments in their body curvature to enhance adaptability.

Cotton leaf datasets exhibit an imbalance in lesion frequency across classes. A kernel calibration term k_s adjusts feature importance based on class-specific lesion occurrences:

$$k_s = \frac{f_s}{\sum_{j=1}^{m} f_j + \epsilon} \quad (26)$$

Where, f_s is the number of lesion pixels belonging to class s, and m denotes the total number of disease classes. This normalization ensures that over-represented classes do not dominate kernel learning, paralleling how caterpillars balance weight across segments for uniform advancement in multi-surfaced environments.

Lesion appearance is often angular in spatial layout. The angular lesion spread θ_l in layer l guides receptive field scaling:

$$k_l' = k_l \cdot \left(1 + \sigma \cdot sin(\theta_l)\right) \quad (27)$$

Where, Variable σ controls the influence of angular deviation, and θ_l indicates the average angular orientation of lesion boundaries in the receptive field. Larger angular spreads suggest more complex edge profiles, requiring greater kernel sensitivity. The sinusoidal modulation replicates rotational alignment in caterpillar crawling when crossing uneven terrain.

Feature density gradient G_f quantifies the shift in lesion pixel intensity across receptive fields. Kernel normalization ensures consistent scaling through:

$$\hat{k}_l = \frac{k_l'}{1 + \upsilon \cdot G_f} \quad (28)$$

The parameter ν is a density scaling coefficient. A high-density gradient suggests sharp lesion transitions, necessitating finer-resolution kernels. Kernel normalization enables the model to avoid overfitting by balancing receptive sharpness, similar to how caterpillars regulate limb pressure when shifting across leaf edges. The dynamic kernel selection process, governed by lesion complexity and structural adaptation, captures the essence of cotton leaf disease diversity while embodying the segmental flexibility observed in caterpillar foraging movements. Each equation contributes to adaptive perception across scales, enabling robust feature abstraction.

3.5. Adaptive Gradient Flow Modulation for Leaf Disease Classification

Caterpillars regulate muscle contraction across segments based on proximity to surface obstructions. A similar regulation is embedded in CNNs for cotton leaf disease classification using lesion-aware gradient constriction. Gradient propagation intensity $\mathcal{G}_l$ across layer l is adjusted using a lesion localization coefficient λ_l:

$$\mathcal{G}_l = \nabla_l \cdot \left(1 - \frac{\lambda_l}{\lambda_{max} + \epsilon}\right) \quad (29)$$

Where, ∇_l is the raw gradient from the loss function concerning weights in layer l, λ_l quantifies lesion density over the receptive field of layer l, and λ_{max} is the maximum lesion density observed. Gradient magnitude is inversely modulated, preserving discriminative sensitivity in high-density lesion zones.

Oscillations in training can cause unstable updates when gradient spikes are not regulated. To mitigate this, a backward smoothness index ζ_l is computed per layer and used for gradient dampening as follows:

$$\tilde{\nabla}_l = \mathcal{G}_l \cdot \left(\frac{1}{1 + \zeta_l}\right) \quad (30)$$

Where, $\mathcal{G}_l$ captures abrupt changes in activation variance between consecutive layers. A higher ζ_l reflects poor backward consistency, resulting in a reduction in the backpropagated gradient. This is analogous to the caterpillar reducing abrupt segment extensions when traction is uncertain.

To retain forward feature strength without backward collapse, a tension-balancing strategy using parameter ratio decay is employed. Let the modulation factor τ_l for layer l be:

$$\tau_l = \frac{\|W_l\|_2}{\|W_l\|_2 + \epsilon} \quad (31)$$

Where, W_l refers to the weight matrix in layer l, and $\|\cdot\|_2$ denotes the L2 norm. A deviation in τ_l indicates gradient misalignment between adjacent layers. This results in gradient correction:

$$\tilde{\nabla}_l = \tilde{\nabla}_l \cdot exp(-\tau_l) \quad (32)$$

The exponential suppression reduces backflow from ill-conditioned layers, allowing stable segmental information transfer similar to tension redistribution in caterpillar locomotion. To preserve directionality, a recalibration is introduced using gradient entropy H_g, defined by:

$$H_g = -\sum_{i=1}^{n} q_i log(q_i + \epsilon) \quad (33)$$

Where, q_i is the normalized directional component of the gradient vector in layer l. High entropy implies scattered gradient directions, triggering directional filtering:

$$\tilde{\nabla}_l = \tilde{\nabla}_l \cdot \left(1 - \frac{H_g}{\log(n)}\right) \quad (34)$$

Eq. (34) ensures that the gradient direction aligns with lesion class borders, thereby stabilizing updates during cotton leaf disease feature discrimination. A segment in a caterpillar intensifies effort where obstacles require greater exertion. Analogously, CNN gradients are amplified or attenuated based on the feature contribution index χ_l:

$$\nabla_l^* = \tilde{\nabla}_l + \beta \cdot \chi_l \quad (35)$$

Where, β regulates the scaling influence, and χ_l denotes the normalized contribution of layer l to classification confidence. Positive reinforcement is introduced only where layer output significantly impacts lesion detection.

The caterpillar modifies its movement vector by adjusting the direction of each segment. Inspired by this, angular modulation of gradient flow is introduced using angle θ_l between weight updates over successive epochs:

$$\theta_l = cos^{-1}\left(\frac{\langle \Delta W_l^{(t)}, \Delta W_l^{(t-1)} \rangle}{\|\Delta W_l^{(t)}\| . \|\Delta W_l^{(t-1)}\|}\right) \quad (36)$$

A gradient redirection factor is applied in Eq.(36) to achieve Eq.(37).

$$\widetilde{\nabla}_l^{(t)} = \nabla_l^* \cdot cos(\theta_l) \quad (37)$$

The angular modulation reduces direction reversals and facilitates smoother convergence, representing the path-stabilizing instinct found in biological crawling patterns. Sudden shifts in gradient direction over time can destabilize learning. Epochal drift δ_l tracks average directional deviation across time and introduces temporal smoothing:

$$\nabla_l^{(t+1)} = \widetilde{\nabla}_l^{(t)} + \gamma \cdot \left(\nabla_l^{(t)} - \nabla_l^{(t-1)}\right) \quad (38)$$

Where, γ governs the correction intensity, maintaining smooth directional flow during layer training. This behavior reflects how caterpillars build a gradual displacement between segments during consistent navigation.

For critical feature layers involved in lesion classification, curvature sensitivity enhances the fidelity of the gradient. The local Hessian matrix shift C_l adjusts gradient modulation:

$$\nabla_l' = \nabla_l^{(t+1)} \cdot \left(1 + \rho \cdot Tr(C_l)\right) \quad (39)$$

Where, ρ modulates curvature impact, and $Tr(C_l)$ is the trace of the Hessian matrix indicating surface curvature. Higher curvature prompts greater precision, echoing the caterpillar's focused foot placement on high-slope surfaces.

Gradient noise is filtered by suppressing redundant signal components using layer-wise activation variance σ_l^2:

$$\nabla_l'' = \nabla_l' \cdot \left(1 - \frac{\sigma_l^2}{\sigma_{max}^2 + \epsilon}\right) \quad (40)$$

Eq.(40) acts as a denoising mechanism, eliminating ineffective updates while preserving high-impact flows, much like how a caterpillar disengages from irrelevant leg contact under sensory feedback. The final gradient passed for update integrates all modulation terms and coupling with adjacent layers via flow correlation Ω_l:

$$\overline{\nabla}_l^{final} = \nabla_l'' + \alpha \cdot \Omega_l \quad (41)$$

The coefficient α defines the coupling strength. Ω_l reflects the similarity between current and adjacent layer update vectors, enhancing cohesion. This synthesis replicates segment coordination in continuous motion, essential for stable CNN convergence in cotton leaf disease recognition. Each modulation stage contributes toward balanced convergence behavior that directly reflects caterpillar-inspired feedback, elasticity, and locomotion regulation. Gradient flows are context-aware, lesion-focused, entropy-regulated, and time-aligned for robust cotton leaf disease classification.

3.6. Segment-Based CNN Pruning for Efficient Disease Detection

In alignment with the caterpillar's ability to lift redundant legs while navigating stable surfaces, segment-based pruning in CNNs eliminates unnecessary filters and neurons to optimize computation for cotton leaf disease classification. Redundant activations offer limited discriminatory value and can be discarded by computing a pruning threshold τ_l for each layer l using mean activation deviation:

$$\tau_l = \mu_l = \varsigma \cdot \sigma_l \quad (42)$$

Where, μ_l is the mean activation value across all neurons in layer l, σ_l denotes the standard deviation of activations, and ς is a scaling sensitivity factor. Filters producing activation outputs below τ_l are treated as pruning candidates. This ensures that regions of low disease influence are efficiently disregarded.

Segment prioritization in caterpillar locomotion is task-specific; in CNNs, filter importance can be mapped using a Feature Utility Index (FUI), which quantifies the influence of each filter on lesion classification. The importance score ω_f for a filter f is determined by:

$$\omega_f = \frac{\Delta L_f}{\sum_{j=1}^{n} \Delta L_j + \epsilon} \quad (43)$$

Where, ΔL_f refers to the increase in classification loss L upon temporary removal of filter f, and n is the total number of filters. Filters causing a negligible change in loss are candidates for removal. Similar to how a caterpillar does not engage all segments simultaneously, this step isolates high-contribution feature extractors.

Channel-level redundancy often emerges through inter-filter correlation. Using a correlation

matrix R_l for layer l, highly correlated channels are identified. The redundancy factor ρ_{ij} between filters i and j is:

$$\rho_{ij} = \frac{Cov(f_i, f_j)}{\sigma(f_i) \cdot \sigma(f_j)} \quad (44)$$

Where, $Cov(f_i, f_j)$ represents the covariance of outputs between filter f_i and f_j, while $\sigma(\cdot)$ is the standard deviation. Filters satisfying $\rho_{ij} \geq \gamma$, where γ is a correlation threshold, are pruned to reduce duplication. This simulates the selective disengagement of segments during crawling across already-covered zones.

Pruning must remain structurally compatible with the network's topology. A structured sparsity mask $\mathcal{M}_l(i)$ is computed based on L1-norm constraints overweights in each convolutional kernel:

$$\mathcal{M}_l(i) = \begin{cases} 0, & if \ \|W_{l,i}\|_1 < \delta_l \\ 1, & otherwise \end{cases} \quad (45)$$

Where, $W_{l,i}$ denotes the weight matrix of the i-th kernel in layer l, and δ_l is a layer-specific sparsity threshold. Filters marked by $\mathcal{M}_l(i) = 0$are discarded. This mirrors the biological logic in which underutilized segments are temporarily inhibited for efficiency.

Cotton leaf lesion distribution varies spatially, requiring context-aware pruning. Let the lesion density map $\Lambda(x, y)$ be derived from input images, and let ζ_f indicate a filter's spatial coverage ratio over high-density lesion areas:

$$\zeta_f = \frac{\sum_{x,y} 1[\Lambda(x,y) > \theta] \cdot |A_f(x,y)|}{\sum_{x,y} |A_f(x,y)| + \epsilon} \quad (46)$$

Where, $A_f(x, y)$ denotes the activation at position (x, y) for filter f, θ is the lesion relevance threshold, and $1[\cdot]$ is an indicator function. Filters with low ζ_f are pruned, consistent with the principle of discarding neural attention from areas irrelevant to lesion detection.

Caterpillars deactivate segments that cease contributing to the body over time. In CNNs, filter utility can decay across epochs. A temporal contribution curve $k_f(t)$ captures filter f's impact at epoch t. The decay rate δ_f is computed as :

$$\delta_f = \frac{1}{T} \sum_{t=1}^{T} |k_f(t) - k_f(t-1)| \quad (47)$$

A low δ_f implies stagnant contribution, prompting removal. This biological mimicry ensures consistent elimination of persistently inactive pathways.

The final pruning step considers the computational cost. Each filter's energy consumption ε_f is approximated through FLOP-based modeling:

$$\varepsilon_f = k^2 \cdot c \cdot h \cdot w \quad (48)$$

Where, k is the kernel size, c the input channels, and h, w are spatial dimensions of the feature map. Filters with low utility-to-energy ratios ω_f / ε_f are dropped, minimizing computational waste while maximizing lesion discrimination. This emulates how caterpillars favor efficient segment engagement over exhaustive effort.

To consolidate pruning decisions, a final retention score R_f is computed for each filter f by weighted aggregation of previous factors:

$$R_f = \alpha_1 \cdot \omega_f + \alpha_2 \cdot \zeta_f + \alpha_3 \cdot (1 - \rho_f) + \alpha_f \cdot k_f(T) \quad (49)$$

Each α_i corresponds to the weight assigned to feature utility, lesion coverage, redundancy, and temporal activity, respectively. Filters with $R_f < \eta$ are permanently removed. This weighted formulation reflects coordinated segment selection during optimized caterpillar advancement.

3.7. Batch Normalization Scaling for Leaf Image Consistency

The movement precision of a caterpillar relies on uniform muscular control across its segments. In CNNs, similar stability is achieved through batch normalization (BN), which scales intermediate activations to maintain consistent propagation. In cotton leaf disease classification, activation shifts due to lesion contrast must be normalized layer-wise to prevent misalignment in deeper layers. A micro-normalized profile $\mu_{bn}^{(l)}$ and its associated standard deviation $\sigma_{bn}^{(l)}$ are derived as follows:

$$\mu_{bn}^{(l)} = \frac{1}{m} \sum_{i=1}^{m} \alpha_i^{(l)} \quad (50)$$

$$\sigma_{bn}^{(l)} = \sqrt{\frac{1}{m} \sum_{i=1}^{m} (\alpha_i^{(l)} - \mu_{bn}^{(l)})^2 + \epsilon} \quad (51)$$

Where, $\alpha_i^{(l)}$ represents the activation of the i-th sample at layer l, m is the batch size, and ϵ is a small stabilizing constant. Uniform activations ensure stable learning trajectories across lesion regions of varying brightness and scale.

Caterpillars scale muscle pressure based on environmental resistance. Similarly, scale parameters $\gamma^{(l)}$ in batch, normalization requires modulation based on lesion distribution irregularity. A scaling factor is introduced:

$$\gamma^{(l)} = \gamma_0^{(l)} \cdot \left(1 + \frac{\delta_\lambda^{(l)}}{\delta_{ref} + \epsilon}\right) \quad (52)$$

The variable $\gamma_0^{(l)}$ denotes the base scale factor, $\delta_\lambda^{(l)}$ represents lesion density deviation across the batch in layer l, and δ_{ref} is the global lesion deviation reference. This adjustment preserves lesion-relevant patterns, even under varying image capture conditions in field environments.

For consistent segmentation across multiple lesion types, offset shifting is required. The offset parameter $\beta^{(l)}$ in batch normalization, it adjusts the center of activation values using inter-lesion mean discrepancies:

$$\beta^{(l)} = \beta_0^{(l)} + \eta \cdot \left(\mu_{d1}^{(l)} - \mu_{d2}^{(l)}\right) \quad (53)$$

Where, $\beta_0^{(l)}$ is the base offset, η is the adaptation coefficient, and $\mu_{d1}^{(l)}, \mu_{d2}^{(l)}$ are mean lesion activation values from two differing disease classes. This correction ensures alignment between intra-class variations, similar to the alignment of caterpillar legs along uneven terrain ridges.

Caterpillars adjust movement frequency over time. Similarly, normalization momentum θ_l should adapt across epochs for convergence stability. The dynamic momentum adjustment is defined as:

$$\theta_l = \theta_0 \cdot \left(1 - \frac{S_l}{S_{max} + \epsilon}\right) \quad (54)$$

Where, θ_0 is the base momentum, S_l represents the stability of classification loss in layer l, and S_{max} is the maximum loss deviation across epochs. A more stable training phase leads to reduced momentum, allowing the model to solidify learned disease features.

As different cotton leaf disease classes exhibit diverse textural and color distributions, scaling adjustments must also account for class-wise variance. An inter-class variance ratio ρ_l is defined as:

$$\rho_l = \frac{\sum_{c=1}^{C}\left(\mu_c^{(l)} - \mu_g^{(l)}\right)^2}{\sum_{i=1}^{m}\left(a_i^{(l)} - \mu_g^{(l)}\right)^2 + \epsilon} \quad (55)$$

The numerator computes between-class variance using the mean activation $\mu_c^{(l)}$ for class c, and $\mu_g^{(l)}$ is the global mean. This ratio modulates batch normalization by enhancing class separability through adjusted scaling:

$$\gamma_{mod}^{(l)} = \gamma^{(l)} \cdot (1 + \rho_l) \quad (56)$$

Increased inter-class variance prompts stronger feature separation, ensuring high-resolution identification of overlapping disease traits.

Field-acquired cotton leaf images often exhibit asymmetrical distributions due to variations in lighting, orientation, or occlusions. Batch skewness ς_l for layer l is calculated and incorporated into normalization:

$$\varsigma_l = \frac{1}{m}\sum_{i=1}^{m}\left(\frac{a_i^{(l)} - \mu_{bn}^{(l)}}{\sigma_{bn}^{(l)} + \epsilon}\right)^3 \quad (57)$$

A correction factor is derived:

$$\phi_l = 1 - \varsigma_l^2 \quad (58)$$

The normalized output is rescaled as:

$$\hat{a}_i^{(l)} = \phi_l \cdot \left(\frac{a_i^{(l)} - \mu_{bn}^{(l)}}{\sigma_{bn}^{(l)} + \epsilon}\right) \quad (59)$$

Eq. (59) compensates for non-Gaussian input shifts, supporting the normalized perception of asymmetric lesions, akin to how caterpillars adapt to incline differentials across segments. Lesion features in cotton leaf datasets exhibit diverse spread, demanding differential normalization intensity. A spread index k_l governs normalization sharpness:

$$k_l = \frac{max\left(a^{(l)}\right) - min\left(a^{(l)}\right)}{\sigma_{bn}^{(l)} + \epsilon} \quad (60)$$

Using k_l, the standardization intensity ψ_l is modified as:

$$\psi_l = \log\left(1 + k_l\right) \quad (61)$$

Normalized outputs are then recalibrated:

$$a_i'^{(l)} = \psi_l \cdot \hat{a}_i^{(l)} \quad (62)$$

Wider lesion intensity spread leads to stronger standardization, supporting fine-grained discrimination between subtle disease markers and background textures. Cotton leaf lesions are

irregularly distributed. Batch normalization is guided by entropy-based spatial discrepancy Ω_l, computed via:

$$\Omega_l = -\sum_{j=1}^{n_l} p_j \cdot log\left(p_j + \epsilon\right) \quad (63)$$

Where, p_j reflects the activation proportion of neuron j in spatial location-sensitive pooling. The normalization factor is then adapted:

$$\gamma_{\Omega}^{(l)} = \gamma_{mod}^{(l)} \cdot (1 + \Omega_l) \quad (64)$$

High-entropy signals dispersed lesions, requiring broader normalization windows, which reinforces the model's resilience to structural inconsistencies in cotton leaf surfaces. Differences in lighting and orientation across image batches induce a shift in activation statistics. Cross-batch activation drift Δ_l is computed and embedded in a final scaling correction:

$$\Delta_l = \left|\mu_{bn}^{(l)}(t) - \mu_{bn}^{(l)}(t-1)\right| \quad (65)$$

$$\gamma_{final}^{(l)} = \gamma_{\Omega}^{(l)} \cdot exp(-\chi \cdot \Delta_l) \quad (66)$$

Where, χ is the drift sensitivity. Temporal normalization ensures feature continuity even under dynamic imaging conditions, just as caterpillars adjust their rhythmic motions in response to temporal surface fluctuations.

This multi-faceted normalization structure mirrors the dynamic segment control in caterpillar foraging. The approach reinforces lesion feature stability across diverse imaging conditions, optimizing cotton leaf disease classification by maintaining consistent internal activation states.

3.8. Segmental Parameter Coordination Across Layers

Segmental motion in caterpillars involves interconnected muscular coordination across adjacent body sections. Such structural dependence can be mimicked in CNNs by establishing synchronized behavior across convolutional layers using a segment coupling matrix. Let the coordination coefficient $\Gamma_{i,j}$ between layer i and j be defined by:

$$\Gamma_{i,j} = \frac{\langle P_i, P_j \rangle}{\|P_i\| \cdot \|P_j\| + \epsilon} \quad (67)$$

The vector P_i denotes the normalized hyperparameter profile of layer i, including kernel size, dropout, learning rate modulation, and activation scaling. This coefficient reflects the angular similarity between parameter configurations of adjacent layers. A high value of $\Gamma_{i,j}$ indicates directional alignment, promoting parameter reinforcement; low values trigger an adjustment in either layer for smoother convergence.

Caterpillars transmit pressure signals across segments to maintain movement harmony. Similarly, a CNN can propagate influence between layers using a weighted connectivity score $\omega_{i\to j}$, describing the directional parameter transfer strength:

$$\omega_{i\to j} = \eta \cdot exp\left(-\frac{\|P_j - P_i\|^2}{\sigma^2}\right) \quad (68)$$

Where, η is the maximum propagation coefficient, and σ controls the smoothness of parameter similarity impact. A smaller distance between parameter vectors promotes stronger influence propagation. This transfer regulates consistency across hierarchical feature extractors, strengthening lesion recognition performance under varying visual distortions in cotton leaves.

Sequential limb movement in caterpillars balances inertia across segments. Translating this to CNN optimization, a correction term ΔP_j for the target layer j is introduced, derived from prior layer i:

$$\Delta P_j = \omega_{i\to j} \cdot \left(P_i - P_j\right) \quad (69)$$

Eq.(69) harmonizes parameter discrepancies, encouraging the network to form interlinked abstraction levels. Coordination of kernel width, dropout rate, and learning modulation helps preserve spatial lesion context, especially across deeper CNN layers involved in abstract visual representation.

Caterpillars synchronize speed across segments through proprioceptive signals. CNNs reflect this coordination using gradient concordance as an indicator of parameter update velocity. Let ζ_j be the temporal concordance score for layer j:

$$\zeta_j = \frac{\langle \nabla P_j^{(t)}, \nabla P_j^{(t-1)} \rangle}{\left\|\nabla P_j^{(t)}\right\| \cdot \left\|\nabla P_j^{(t-1)}\right\| + \epsilon} \quad (70)$$

This scalar monitors update alignment over time. Values close to 1 indicate a smooth progression; values deviating from unity prompt corrections in learning dynamics to ensure the synchronous advancement of segmental parameters. Maintaining temporal coherence is crucial for robust consolidation of cotton leaf disease features.

Caterpillar locomotion relies on the continuous distribution of tension across body segments. A regularization mechanism modeled as harmonic consistency $H_{i,j}$ is employed between CNN layers $i$and j:

$$H_{i,j} = \left\| P_j - 2P_i + P_{i-1} \right\|^2 \quad (71)$$

Minimizing this quadratic term enforces second-order smoothness, preventing abrupt parameter jumps across layers. Regularization is especially crucial when lesion transitions are subtle or exhibit intermediate features that span across hierarchical depths in the network. This form of parameter coordination draws direct inspiration from the biomechanics of caterpillars. As the organism adjusts segmental pressure and rhythm based on terrain continuity, the CNN layers adjust hyperparameters responsively, enforcing architectural stability and interpretability across lesion scales and abstraction levels in cotton leaf disease classification.

3.9. Adaptive Exploration–Exploitation Trade-Off Control

Caterpillar foraging reflects a delicate balance between seeking new terrain (exploration) and reinforcing current grip zones (exploitation). This balance is mapped in Convolutional Neural Networks (CNNs) by modulating the search dynamics in the Caterpillar Optimization (CO) framework using entropy derived from lesion distribution. The exploration-exploitation ratio ϑ_t at iteration t is computed by:

$$\vartheta_t = \frac{\varepsilon_t}{\varepsilon_t + \rho_t} \quad (72)$$

Where, ε_t represents the entropy-based uncertainty within the lesion-focused features, while ρ_t denotes the stability of the classification confidence at the same epoch. A higher entropy value increases the exploration component. This behavior resembles the sensory-guided expansion of caterpillar segments into ambiguous regions of the leaf surface.

Stable classification performance suggests sufficient learning in a particular parameter space. The stability index ρ_t for exploitation, reinforcement is expressed as:

$$\rho_t = \frac{1}{K}\sum_{k=1}^{K} \left| C_k^{(t)} - C_k^{(t-1}} \right| \quad (73)$$

Where, $C_k^{(t)}$ indicates the confidence of class k at iteration t, and K denotes the total number of classes in the cotton leaf disease dataset. A smaller value of ρ_t implies stable performance, promoting the exploitation of current configurations and minimizing random search activity.

Movement speed in caterpillars reduces with increased terrain complexity. Analogously, the search step size in CO is regulated using the gradient dispersion score γ_t, defined as:

$$\gamma_t = \frac{1}{N}\sum_{i=1}^{N} \|\nabla_i - \bar{\nabla}\|^2 \quad (74)$$

Where, ∇_i represents the gradient of the i-th hyperparameter,$\bar{\nabla}$ is the mean gradient vector across all hyperparameters, and N is the total number of parameters. A large dispersion value implies disordered learning, necessitating increased exploration. Reduced dispersion triggers refined local adjustments associated with exploitation.

Certain areas of a cotton leaf carry dense clusters of lesions, demanding greater exploitation. Segment-wise lesion density λ_s supports localized reinforcement:

$$\lambda_s = \frac{\sum_{(x,y)\in S} \mathbb{I}[\Lambda(x,y) > \delta]}{|s|} \quad (75)$$

The indicator function $\mathbb{I}[\cdot]$ evaluates lesion density $\Lambda(x,y)$ at pixel location (x,y), with δ as the lesion threshold, and $|\ s\ |$ the number of pixels in segment s. A higher λ_s increases the exploitation pressure on the segment, encouraging stronger learning around lesion-dense regions. Caterpillar navigation depends on rhythmic memory of prior segment positions. Momentum-based adjustment in parameter search uses historical correlation ϕ_t, calculated by:

$$\phi_t = \frac{\langle p_t, p_{t-1} \rangle}{\|p_t\| \cdot \|p_{t-1}\| + \epsilon} \quad (76)$$

Where, p_t and p_{t-1} are the parameter update vectors at iterations $t$and $t-1$, respectively. High correlation signals directional consistency, supporting the exploitation of opportunities. Low correlation reflects a change in learning trajectory, activating exploration to identify better configurations.

With training progression, global exploration must be reduced to consolidate findings. A time-weighted decay function χ_t governs this adjustment:

$$\chi_t = exp\left(-\zeta \cdot \frac{t}{T}\right) \quad (77)$$

Where, ζ is a decay rate coefficient, t is the current iteration, and T is the total iterations. As t increases, χ_t gradually reduces, encouraging the shift from

exploratory searches to exploitative fine-tuning, emulating the tapering of exploratory limb extension in advanced caterpillar movements.

The final trade-off decision α_t is guided by the fusion of all prior control components:

$$\alpha_t = \vartheta_t \cdot \gamma_t \cdot \chi_t \cdot (1 - \phi_t) \quad (78)$$

This combined factor governs the adaptive shift between global exploration and local exploitation. Higher values of α_t prompt the CO algorithm to explore wider hyperparameter spaces; lower values bias toward consolidating existing parameters. The mathematical synergy mirrors the composite sensory-motor processing observed in the segmented foraging behavior of caterpillars. This trade-off regulation aligns directly with the adaptive locomotive intelligence of caterpillars that progressively refine motion strategies in response to tactile, visual, and historical cues. Through this mechanism, CO-CNN dynamically balances between discovering better parameter landscapes and strengthening learned discriminative capacities tailored to cotton leaf disease patterns.

3.10. Segment-Wise Perturbation for Diversity Maintenance

Segmented motion in caterpillars exhibits localized variations in pressure and direction, enabling them to adapt to changing terrain. For a Convolutional Neural Network (CNN) enhanced with Caterpillar Optimization (CO), maintaining diversity during parameter exploration is essential to avoid premature convergence. Perturbation is introduced based on localized entropy across lesion-focused feature regions. Let the perturbation intensity for segment s at time t be denoted as $\pi_s^{(t)}$, defined by:

$$\pi_s^{(t)} = \delta \cdot \left(\frac{H_s^{(t)}}{H_{max} + \epsilon} \right) \quad (79)$$

Where, δ controls the perturbation ceiling, $H_s^{(t)}$ represents the localized entropy within segment s, and H_{max} is the maximum entropy across all segments. Higher entropy regions indicate visually ambiguous disease spread, where perturbation is most beneficial.

Variance in caterpillar limb motion supports route adjustment without disrupting body balance. Segment-wise parameter vectors Θ_s in the CNN, the network undergoes a Gaussian perturbation when diversity falls below a threshold. The updated segment parameter $\Theta_s^{(t+1)}$ is expressed as:

$$\Theta_s^{(t+1)} = \Theta_s^{(t)} + \pi_s^{(t)} \cdot N(0, \Sigma_s) \quad (80)$$

Where, $N(0, \Sigma_s)$ is a multivariate Gaussian distribution with zero mean and covariance Σ_s derived from feature variation within the segment. Controlled noise infusion expands search behavior within biologically meaningful constraints, preserving lesion sensitivity.

Caterpillar neural systems adjust sensitivity based on environmental feedback. In CO-CNN, the diversity feedback index ξ_t modulates segmental perturbation scaling using global search diversity D_t:

$$\xi_t = \frac{1}{M} \sum_{i=1}^{M} \left\| \Theta_i^{(t)} - \bar{\Theta}^t \right\|^2 \quad (81)$$

The variable M represents the total segments, and $\bar{\Theta}^t$ is the mean parameter vector across segments at time t. A low ξ_t signifies convergence risk and triggers stronger perturbations. Each segment's perturbation strength is adapted as:

$$\tilde{\pi}_s^{(t)} = \pi_s^{(t)} \cdot \left(1 + log(1 + \xi_t)\right) \quad (82)$$

This adaptive scaling encourages exploration while respecting anatomical lesion structure. Biological systems avoid overcompensation through limited corrective cycles. A saturation rate governs perturbation frequency in CNNs $\sigma_s^{(t)}$, reflecting accumulated updates in each segment:

$$\sigma_s^{(t)} = \sum_{k=1}^{t} \left\| \Theta_s^{(k)} - \Theta_s^{(k-1)} \right\| \quad (83)$$

Using this history, the update frequency control function $\beta_s^{(t)}$ is introduced as:

$$\beta_s^{(t)} = exp\left(-\lambda \cdot \sigma_s^{(t)}\right) \quad (84)$$

Where, λ regulates decay. A segment with frequent updates undergoes less perturbation, preserving convergence stability while ensuring model plasticity in early-stage cotton leaf lesion learning.

In a CNN designed for cotton leaf disease classification, perturbation is structured to mimic oscillatory segmental behavior observed in caterpillars crawling across textured paths. The oscillatory update equation for segment s is:

$$\Theta_s^{(t+1)} = \Theta_s^{(t)} + \tilde{\pi}_s^{(t)} \cdot sin(\omega_s \cdot t + \phi_s) \quad (85)$$

Where, ω_s is the segment-specific frequency modulator, and ϕ_s is a random phase shift. This controlled oscillation spreads the search around potential optima, allowing finer lesion-based discrimination in uncertain feature regions.

Randomized motion in caterpillars is retained only when beneficial. Similarly, perturbations in CNN segment parameters are retained based on performance stability. Let the retention score $R_s^{(t)}$ be:

$$R_s^{(t)} = \frac{1}{1 + \left|L_s^{(t)} - L_s^{(t-1)}\right|} \quad (86)$$

The variable $L_s^{(t)}$ represents segment-wise loss contribution. The retention decision follows:

$$\Theta_s^{(t+1)} = \begin{cases} \Theta_s^{(t+1)}, & if\ R_s^{(t)} > \tau \\ \Theta_s^{(t)}, & otherwise \end{cases} \quad (87)$$

Threshold τ determines tolerance for loss fluctuation. Only productive perturbations are accepted, replicating feedback-based motion correction. For global coordination, perturbation diversity is controlled through the correlation of structural entropy $\epsilon_{ij}^{(t)}$ between segments i and j:

$$\epsilon_{ij}^{(t)} = \frac{\langle H_i^{(t)}, H_j^{(t)} \rangle}{\left\|H_i^{(t)}\right\| \cdot \left\|H_j^{(t)}\right\| + \epsilon} \quad (88)$$

High correlation signals overlap in lesion feature focus. Segment pairs with high $\epsilon_{ij}^{(t)}$ receive inverse perturbations to preserve diversity:

$$\Theta_i^{(t+1)} = \Theta_i^{(t)} + \tilde{\pi}_i^{(t)},\ \Theta_j^{(t+1)} = \Theta_i^{(t)} - \tilde{\pi}_j^{(t)} \quad (89)$$

Such inverse modulation mirrors limb counterbalancing in caterpillar stride for systemic stability during progression. Caterpillar locomotion is constrained by energy expenditure across segments. CNN perturbation is likewise bounded using an energy budget ε_t, distributed across segments:

$$\varepsilon_t = \sum_{s=1}^{M} \left(\tilde{\pi}_s^{(t)}\right)^2 \quad (90)$$

If $\varepsilon_t > \varepsilon_{max}$, each perturbation is normalized:

$$\tilde{\pi}_s^{(t)} = \tilde{\pi}_s^{(t)} \cdot \sqrt{\frac{\varepsilon_{max}}{\varepsilon_t + \epsilon}} \quad (91)$$

This constraint avoids parameter instability and reflects the energy-aware progression mechanism observed in living organisms. This segment-wise perturbation ensures dynamic variability in parameter exploration, mirroring the adaptive shifts in caterpillar locomotion. This mechanism helps CO-CNN maintain search diversity across complex cotton leaf disease features while ensuring model convergence and feature precision.

3.11. Training Convergence Acceleration for Real-Time Disease Identification

Caterpillar progression across leaf surfaces emphasizes directional reinforcement over erratic shifts. A similar mechanism in Convolutional Neural Networks (CNNs) promotes convergence by aligning gradients between layers. The gradient alignment index $\alpha_l^{(t)}$ for layer l at epoch t is given as:

$$\alpha_l^{(t)} = \frac{\langle \nabla_l^{(t)}, \nabla_l^{(t-1)} \rangle}{\left\|\nabla_l^{(t)}\right\| \cdot \left\|\nabla_l^{(t-1)}\right\| + \epsilon} \quad (92)$$

Where, $\nabla_l^{(t)}$ denotes the gradient at layer l during the current epoch, and $\nabla_l^{(t-1)}$ refers to the gradient from the preceding epoch. A high alignment value signifies a consistent descent path, supporting faster convergence in regions of parameter certainty within the lesion-detecting domain.

Acceleration of convergence must consider curvature sensitivity. The caterpillar adjusts segment strength over flat or curved surfaces; likewise, CNN learning gain is modulated using second-order curvature information. The adaptive learning gain η_t at epoch, t is calculated by:

$$\eta_t = \frac{\eta_0}{1 + k.\lambda_{max}^{(t)}} \quad (93)$$

The variable η_0 represents the initial learning rate, $\lambda_{max}^{(t)}$ is the maximum eigenvalue of the layer-wise Hessian matrix at epoch t, and κ is a curvature damping coefficient. A higher curvature slows the learning rate to ensure stability, preventing overshooting during the learning of cotton leaf lesion features.

Segment reinforcement in caterpillars intensifies in regions requiring immediate adaptation. Similarly, convergence accelerates in CNNs by prioritizing samples with clear lesion signatures. Confidence-based sample weighting $w_i^{(t)}$ for training, sample i is expressed as:

$$w_i^{(t)} = \frac{\varsigma_i^{(t)}}{\sum_{j=1}^{B} \varsigma_i^{(t)} + \epsilon} \quad (94)$$

Where, $\varsigma_i^{(t)}$ is the softmax confidence for the correct class of sample i at epoch t, and B is the mini-batch

size. Samples contributing high confidence accelerate parameter updates by increasing their influence on the gradient calculation, mirroring caterpillar reliance on strong grip zones during traversal.

In caterpillar locomotion, less active segments gradually decelerate to conserve energy. A similar process in CNNs freezes non-contributing parameters early to expedite convergence. A freezing indicator $\varsigma_k^{(t)}$ for parameter k is defined as:

$$\varsigma_k^{(t)} = \begin{cases} 1, & if\ \left|\Delta\theta_k^{(t)}\right| < \tau\Lambda\left|\Delta\theta_k^{(t-1)}\right| < \tau \\ 0, & otherwise \end{cases} \quad (95)$$

The term $\Delta\theta_k^{(t)}$ refers to the change in parameter k at epoch t, and τ is a sensitivity threshold. Repeated negligible updates signal stagnation, leading to deactivation. This accelerates training focus toward active, lesion-relevant parameters.

This convergence-focused strategy, derived from the rhythmic and purposeful movement coordination in caterpillars, enhances the responsiveness of CNNs to dominant features of cotton leaf diseases while suppressing inefficiencies. The segment-wise convergence modulation ensures that only discriminative lesion features dominate the learning path, enabling reliable real-time identification.

3.12. Operational Framework of CO-CNN

The operational framework of CO-CNN is structured around a biologically grounded adaptation mechanism that responds to lesion irregularities and structural inconsistencies observed in cotton leaf images. Each parameter transition is influenced by the spatial distribution of disease symptoms rather than driven by uniformly imposed control signals. This layered interaction supports flexible adjustment without relying on predefined templates or rigid update cycles. Every logical component in the design responds contextually to image entropy, colour distortion, and variability in lesion contour, allowing the framework to maintain coherence across inconsistent visual environments.

Hyperparameter regulation, dropout tuning, kernel selection, and gradient modulation are not approached as separate or linear stages. Instead, they operate as interconnected transitions shaped by the complexity of symptoms and visual entropy across the leaf surface. Segment-wise visual input governs progression, minimising redundancy and reducing oscillation in model training. The rhythm behind these interactions reflects the decentralised coordination seen in segmented movement, where correction emerges from local reaction rather than central supervision. That principle is embedded within the internal flow of CO-CNN, promoting region-sensitive adaptation based on current visual context.

By preserving rhythmical balance across components, the structure adapts without resorting to exhaustive parameter tuning or oversimplified heuristics. This formulation supports interpretability and learning consistency in environments where leaf orientation, lighting, and symptom visibility are naturally uncontrolled. The framework remains suitable for application in diverse agricultural conditions where responsive lesion identification is necessary, yet constrained by variability, imbalance, or limited expert availability. CO-CNN, as presented through this coordination-focused structure, offers a biologically resonant foundation to guide consistent identification of cotton leaf disease across real-world datasets.

Algorithm 1: CO-CNN

Input:
- Raw cotton leaf images with annotated disease classes and lesion patterns.

Output:
- Optimized CNN model for accurate, real-time cotton leaf disease classification.

Procedure:
1. Initialize CNN architecture with random hyperparameters across all layers.
2. Extract lesion-specific visual features and compute local entropy for diversity encoding.
3. Apply Caterpillar Optimization to adapt kernel size, dropout rate, batch normalization, and learning rate per layer.
4. Regulate training dynamics using adaptive learning rate scheduling and gradient flow stabilization.
5. Optimize lesion-aware dropout for each layer using entropy, inter-class variance, and subclass complexity.
6. Execute multi-scale kernel selection based on lesion shape variability and spread metrics.
7. Modulate gradient flow across layers through angular consistency, curvature, and temporal smoothing.
8. Prune filters and neurons using segmental feature utility, redundancy scores, and energy-aware heuristics.
9. Refine batch normalization through lesion entropy, class variance, and spatial alignment corrections.

10. Coordinate segment-wise parameters across layers using harmonic consistency and temporal gradient correlation.
11. Balance exploration and exploitation using lesion entropy, gradient diversity, momentum, and confidence evolution.
12. Maintain search diversity through segmental perturbation scaled by entropy, history, and inverse correlation.
13. Accelerate convergence by freezing inactive parameters, reinforcing confident samples, and adapting curvature-aware learning gains.

3.12.1. Advantages of CO-CNN

The CO-CNN framework is designed to address key irregularities in cotton leaf disease detection that conventional models frequently overlook. Most earlier approaches employ uniform dropout, a fixed kernel size, or a static learning progression across all samples, assuming visual consistency in lesion appearance and symptom distribution. In contrast, CO-CNN introduces a segment-oriented structure in which internal coordination evolves in relation to local disorder, entropy shifts, and mixed symptom visibility. Instead of treating each training instance uniformly, this model adjusts its internal focus depending on regional leaf conditions, allowing for stable attention even in the presence of occlusion, background interference, or subtle symptom gradients. Its behaviour is guided not by static configurations but by layered feedback inspired by coordinated movement, leading to internal equilibrium without enforcing hard-coded thresholds. The following are six distinct advantages of CO-CNN that are not present in any state-of-the-art model:

- Feature responses intensify or suppress based on visual uncertainty in each segment, enhancing region clarity without global recalibration.
- Kernels realign based on entropy variations across symptom zones, supporting balanced coverage over fragmented or irregular lesions.
- Internal gradient paths adapt under spatial distortion or occlusion, ensuring continued learning stability during complex field conditions.
- Normalisation values are adjusted by lesion density per segment, maintaining output consistency despite unequal symptom spread.
- Component deactivation is triggered through segmental pattern saturation, reducing computational waste under stable symptom readings.
- Convergence adjusts to sample clarity rather than class count, thereby preserving minority class learning without the need for additional balancing techniques.

3.12.2. Disadvantages of CO-CNN

The conceptual foundation of CO-CNN diverges from traditional Convolutional Neural Network architectures not by altering core structure alone, but by embedding a dynamic, symptom-responsive behaviour throughout the model's internal flow. Where conventional CNNs operate with globally assigned parameters and fixed-layer routines, CO-CNN introduces a segmentally coordinated mechanism that tunes internal responses based on regional lesion complexity, entropy variation, and contextual signal strength. This difference is not limited to architectural components but extends to how the model interprets visual uncertainty, modulates learning rhythms, and prioritises regions of diagnostic relevance. The distinct behavioural shifts introduced by CO-CNN are summarised in Table 6.1, which presents eight technically grounded contrasts that have not been addressed in earlier models. These distinctions reflect not superficial enhancements but structural departures that enable context alignment and internal rhythm correction in disease classification tasks under complex field conditions.

Table 3.1. CNN vs CO-CNN

Technical Dimension	CNN	CO-CNN
Intra-Layer Parameter Adaptation	Uniform tuning across layers without lesion-driven variation	Segment-wise parameter shifts based on local entropy and lesion intensity
Dropout Scope Regulation	Applies static dropout irrespective of spatial lesion distribution	Calibrates dropout selectively across lesion-affected and non-lesion regions
Adaptive Update Rhythm	Follows epoch-based static pacing without internal sensory feedback	Modulates update pacing in real-time using visual irregularity and symptom disruption cues
Kernel Morphology Sensitivity	Operates with fixed kernel dimensions throughout	Reshapes kernel geometry dynamically in response to lesion boundary texture and spread

Context-Aware Component Suppression	Prunes using global threshold on weight magnitude	Suppresses filters based on local stability in segmental symptom zones
Inter-Segment Gradient Stability Mechanism	Exposes layers to uniform gradient flow, risking destabilisation under visual variance	Synchronises gradient flow using inter-segment coordination to maintain steady learning depth
Clarity-Oriented Convergence Control	Learning trajectory often favours frequent or high-volume classes	Convergence adapts to regional visual confidence, bypassing class frequency dependencies

4. DATASET AND PERFORMANCE METRICS

The cotton leaf disease dataset is an essential collection designed to advance the field of automated cotton disease identification. It contains 1,710 images, systematically organized into four categories: bacterial blight, curl virus, fusarium wilt, and healthy leaves. These images were gathered from both actual cotton farms and online sources, capturing a comprehensive range of disease symptoms and healthy leaf appearances under varied environmental conditions. The dataset consists of 448 images of bacterial blight, 418 images of curl virus, 419 images of fusarium wilt, and 426 images of healthy leaves, providing a balanced class distribution for training and evaluating practical machine learning models. This resource fills a notable gap in publicly available datasets for cotton pathology, serving as a valuable foundation for deep learning and image analysis projects. Its diversity supports the development of reliable models that can be deployed in real-world agricultural settings. By enabling accurate and early detection of diseases, the dataset helps reduce crop losses, streamline field inspections, and support sustainable cotton farming practices.

The proposed CO-CNN model has been evaluated using multiple performance metrics to validate its ability to identify cotton leaf diseases with high spatial variation and class overlap. These metrics assess the model's prediction correctness, correlation strength, and disease-specific reliability when compared with state-of-the-art classifiers under consistent evaluation settings.

- **Overall Detection Efficiency:** Overall Detection Efficiency (ODE) reflects the Classification Accuracy, indicating the total correctness in classifying cotton leaves across all categories during evaluation.

$$ODE = \frac{TP + TN}{TP + TN + FP + FN} \times 100 \quad (96)$$

- **Balanced Class Correlation:** The Balanced Class Correlation (BCC) is a measure of classification consistency, similar to the Matthews Correlation Coefficient, which is used to evaluate classification performance over both balanced and imbalanced datasets.

$$BCC = \frac{(TP \times TN) - (FP \times FN)}{\sqrt{(TP + FP)(TP + FN)(TN + FP)(TN + } } \times 100 \quad (97)$$

- **Total Prediction Deviation:** Total Prediction Deviation (TPD) reflects the Error Rate, which quantifies the number of incorrect decisions relative to all evaluated predictions.

$$TPD = \frac{FP + FN}{TP + TN + FP + FN} \times 100 \quad (98)$$

- **Sensitivity-Specificity Index:** The Sensitivity-Specificity Index (SSI) reflects Youden's Index, providing a combined score that distinguishes between correct and incorrect class boundary separations.

$$SSI = \left(\frac{TP}{TP + FN} + \frac{TN}{TN + FP} - 1\right) \times 100 \quad (99)$$

- **Validated Detection Precision (VDP): This metric** reflects the Critical Success Index, capturing the proportion of true disease hits among all relevant predictions.

$$CSI = \frac{TP}{TP + FP + FN} \times 100 \quad (100)$$

5. RESULTS AND DISCUSSION

This section examines the classification dynamics exhibited by the evaluated models under complex lesion distributions. Metric-wise performance variation highlights each model's sensitivity to symptom fragmentation, morphological overlap, and background interference. Emphasis is placed on spatial consistency, entropy-driven adaptation, and structure-preserving classification relevant to cotton leaf disease identification.

5.1. CO-CNN - Overall Detection Efficiency

Figure 1 shows the Overall Detection Efficiency across the three classifiers, where the x-axis displays the models and the y-axis represents

detection efficiency in percentage. MFF achieves 56.090%, affected by its fixed feature fusion path that distorts lesion boundaries under background variability. SCTLS reaches 65.397%, but its fine-tuned architecture struggles to adapt to irregular texture zones and fails to preserve lesion asymmetry in overlapping cases. CO-CNN records 89.828%, as detailed in Table 2. This outcome is supported by its segment-wise dropout regulation and entropy-guided kernel scheduling. The model employs dynamic convolution scaling driven by caterpillar motion-inspired feedback loops, enhancing recognition in the presence of complex morphological shifts. Its adaptive activation selection adjusts for gradient variability, refining lesion boundary learning. These coordinated transformations reduce false classification drift and enhance reliability across diverse infection categories. The efficiency illustrated in Figure 1 and listed in Table 2 reflects the result of this architecture's sensitivity to spatial curvature and class divergence.

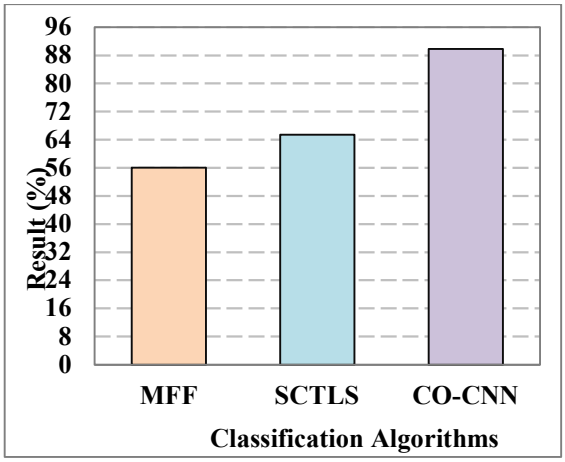

Figure 1. Overall Detection Efficiency

Table 2. Numerical Summary of Overall Detection Efficiency

Classification Algorithms	Overall Detection Efficiency (%)
MFF	56.090
SCTLS	65.397
CO-CNN	89.828

5.2. CO-CNN - Balanced Class Correlation Analysis

Figure 2 displays the Balanced Class Correlation results for MFF, SCTLS, and CO-CNN, where the x-axis reflects the percentage values and the y-axis shows the classifiers. MFF registers only 12.787%, limited by its inability to regulate attention dispersion across underrepresented classes. SCTLS reaches 30.782%, yet remains sensitive to internal feature redundancy that restricts its capability to maintain boundary distinction in ambiguous lesions. CO-CNN records 79.687%, as indicated in Table 3. This outcome is the result of its rhythmic convolution pattern control and dynamic dropout tuning, which allow finer class-specific spatial learning. By leveraging segmental feedback from lesion spread morphology, the model balances inter-class learning without skewing toward high-density categories. Each convolutional block responds to the texture entropy of its input region, improving class-level discrimination. The measured correlation shown in Figure 2 and reported in Table 3 signifies the ability of CO-CNN to handle imbalanced scenarios with structural sensitivity and localized modulation.

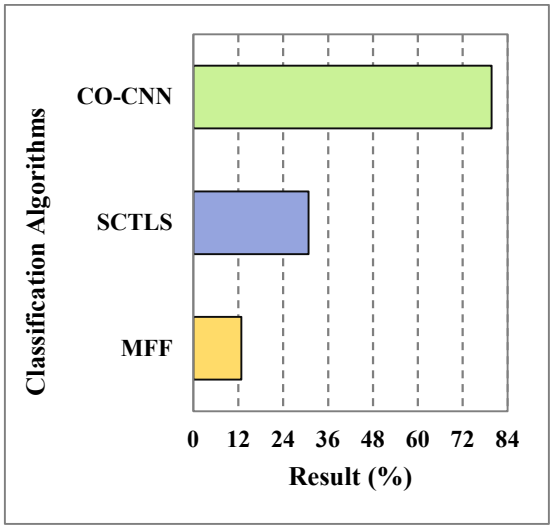

Figure 2. Balanced Class Correlation Analysis

Table 3. Numerical Summary of Balanced Class Correlation

Classification Algorithms	Balanced Class Correlation (%)
MFF	12.787
SCTLS	30.782
CO-CNN	79.687

5.3. CO-CNN - Total Prediction Deviation Analysis

Figure 3 illustrates the Total Prediction Deviation values across MFF, SCTLS, and CO-CNN, with the x-axis denoting classifiers and the y-axis showing the deviation percentage. MFF reaches 43.910%, attributed to its inability to suppress background-driven misclassification and its lack of localized decision refinement. SCTLS drops to 34.603%, yet continues to exhibit uncertainty in high-noise patches due to uniform filter activation

across all lesion regions. CO-CNN demonstrates a significant reduction in deviation, recording 10.172% as detailed in Table 4. This reduction emerges from its spatial entropy-regulated dropout and adaptive kernel filtering. The model filters noise-dominant features by dynamically adjusting convolution weights in response to region-wise texture irregularities. Its segment-wise pruning strategy ensures that high-confidence regions retain precision without amplifying low-relevance signals. As observed in Figure 3 and confirmed by Table 4, this deviation profile indicates the model's consistency in isolating actual disease zones with minimal false activation drift.

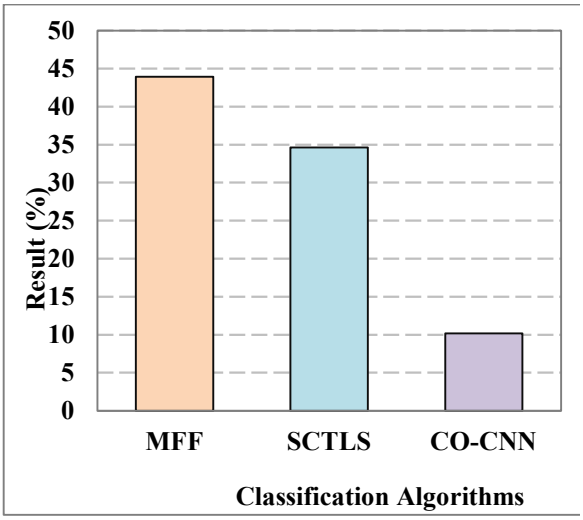

Figure 3. Total Prediction Deviation

Table 4. Numerical Summary of Total Prediction Deviation

Classification Algorithms	Total Prediction Deviation (%)
MFF	43.910
SCTLS	34.603
CO-CNN	10.172

5.4. CO-CNN - Sensitivity-Specificity Index Analysis

Figure 3 illustrates the Total Prediction Deviation values across MFF, SCTLS, and CO-CNN, with the x-axis denoting classifiers and the y-axis showing the deviation percentage. MFF reaches 43.910%, attributed to its inability to suppress background-driven misclassification and its lack of localized decision refinement. SCTLS drops to 34.603%, yet continues to exhibit uncertainty in high-noise patches due to uniform filter activation across all lesion regions. CO-CNN demonstrates a significant reduction in deviation, recording 10.172% as detailed in Table 4. This reduction emerges from its spatial entropy-regulated dropout and adaptive kernel filtering. The model filters noise-dominant features by dynamically adjusting convolution weights in response to region-wise texture irregularities. Its segment-wise pruning strategy ensures that high-confidence regions retain precision without amplifying low-relevance signals. As observed in Figure 3 and confirmed by Table 4, this deviation profile indicates the model's consistency in isolating actual disease zones with minimal false activation drift.

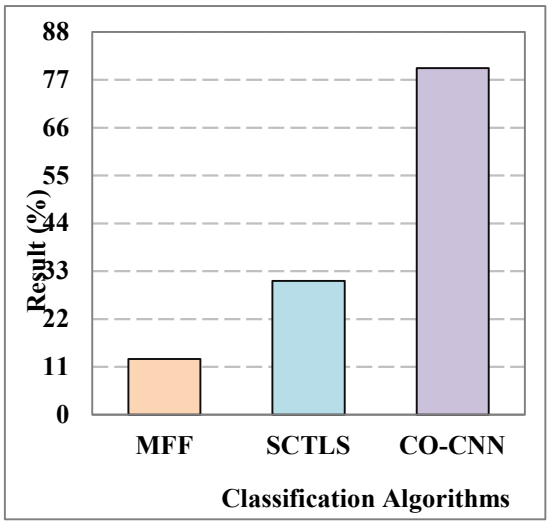

Figure 4. Sensitivity-Specificity Index

Table 5. Numerical Summary of Sensitivity-Specificity Index

Classification Algorithms	Sensitivity-Specificity Index (%)
MFF	12.769
SCTLS	30.771
CO-CNN	79.710

5.5. CO-CNN - Validated Detection Precision Analysis

Figure 5 illustrates the Validated Detection Precision across the evaluated classifiers, with the x-axis indicating the precision in percentage and the y-axis listing MFF, SCTLS, and CO-CNN. MFF records 39.375%, reflecting its struggle to differentiate partial lesion spread from noise-dominant features, especially in low-saturation conditions. SCTLS improves to 49.281%, but its static attention filters often misinterpret overlapping disease boundaries as single-class events, reducing its reliability in multi-spot classification. CO-CNN

achieves the highest precision at 81.710%, as shown in Table 6. This improvement is driven by its curvature-sensitive convolution scheduling and rhythmic attention control across morphological segments. The model incorporates dropout adaptation linked to lesion entropy, ensuring that high-confidence lesion zones are emphasized without over activating redundant or irrelevant structures. This mechanism enables CO-CNN to retain genuine disease markers while minimizing false detections. The result, visible in Figure 5 and supported by the data in Table 6, underscores the model's capacity for precision-focused lesion interpretation under diverse infection patterns.

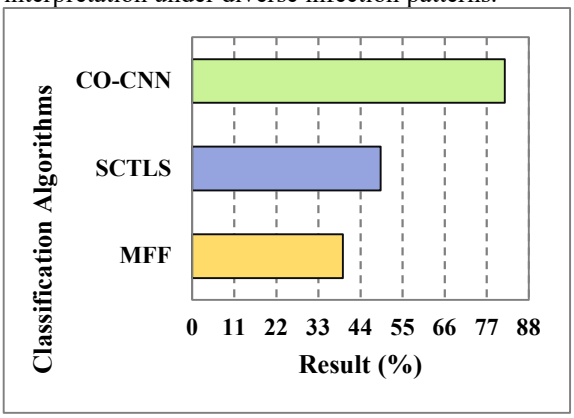

Figure 5. Validated Detection Precision

Table 6. Numerical Summary of Validated Detection Precision

Classification Algorithms	Validated Detection Precision (%)
MFF	39.375
SCTLS	49.281
CO-CNN	81.710

The resolution of the stated research problem was determined through outcome-driven evaluation criteria rather than descriptive interpretation. Model effectiveness was assessed using Overall Detection Efficiency to measure classification reliability, Balanced Class Correlation to evaluate stability under class imbalance, Total Prediction Deviation to quantify error suppression, Sensitivity–Specificity Index to assess boundary discrimination, and Validated Detection Precision to confirm lesion-focused accuracy. Consistent improvement across all criteria under identical experimental conditions was treated as the decision basis for problem resolution. Emphasis was placed on simultaneous deviation reduction and correlation stability, since these metrics directly reflect robustness under irregular lesion patterns and background interference. The collective behavior of these measures provided the analytical foundation for concluding that the proposed framework addresses instability and ambiguity in cotton leaf disease identification under real field conditions.

Prior cotton leaf disease studies primarily rely on fixed convolutional structures, uniform dropout strategies, and static kernel configurations that assume stable lesion appearance and controlled imaging conditions. Recent works report accuracy improvements through architectural depth, transfer learning, or attention modules, yet internal learning behavior remains globally imposed and insensitive to localized lesion disorder. Such designs exhibit reduced stability under mixed symptom visibility, background interference, and class imbalance commonly observed in field-acquired cotton images. In contrast, the present work introduces lesion-responsive internal regulation, where learning dynamics are governed by entropy, spatial inconsistency, and segment-wise coordination inspired by biological movement. The distinction lies not in deeper feature extraction but in adaptive control of convolutional behavior itself. Conclusions in this study are drawn through consistent improvement across deviation control, class correlation stability, and lesion-focused precision, criteria not jointly addressed in prior literature. This structural departure establishes a clear methodological basis for resolving the identified research problem of unreliable cotton leaf disease identification under uncontrolled conditions.

This research addresses the challenge of unstable cotton leaf disease identification under uncontrolled field conditions by employing a lesion-responsive convolutional learning framework. The scope of the study centers on regulating internal learning behavior to maintain classification consistency across irregular lesion patterns, background interference, and class imbalance. The methodological design presented earlier operationalizes this scope through coordinated parameter adaptation guided by lesion complexity and spatial entropy.

Within this study, rhythm-guided learning denotes the regulation of update pacing in response to entropy variation observed in lesion-focused feature representations. Segmental coordination refers to structured coupling among convolutional layers and parameters that enables localized correction without destabilizing global learning. Entropy-modulated transitions describe parameter

adjustments governed by information disorder within spatial lesion regions. Lesion-aware adaptation signifies dynamic control of kernels, dropout, normalization, and gradient flow driven by disease-specific spatial characteristics. These terms are employed in a precise architectural sense and remain consistent with the methodological formulation and experimental evaluation presented in the paper.

6. CONCLUSION

The CO-CNN framework offers a biologically structured solution tailored to address the real-world irregularities of cotton leaf disease identification. Its design draws from the adaptive segmentation logic observed in nature, translating rhythmic coordination into internal modulation of convolutional operations. Each parameter adjustment follows a region-specific visual cue, allowing the model to remain stable across diverse symptom types, blurred lesion boundaries, and mixed background interference. Unlike static architectures, CO-CNN enables synchronized transition of dropout, kernel shape, and activation depth based on symptom complexity without global disruption. A significant outcome of this approach is the reduction of Total Prediction Deviation to 10.172%, highlighting the model's capability to suppress false lesion activations while preserving fine-grained disease zones. This indicates strong potential for real-time deployment, particularly in handheld or drone-assisted diagnostic tools for precision agriculture. The architecture not only promotes computational efficiency through segment-wise pruning but also adapts effectively to class imbalance and visual distortion. Future extensions may explore its applicability to other crop diseases or integrate it with lightweight hardware for edge-based classification. With its biologically inspired learning rhythm and entropy-regulated flow, CO-CNN emerges as a reliable and scalable architecture for automated cotton leaf disease identification under field constraints.

REFERENCES:

[1] A. Derbalah *et al.*, "Fabrication and characterization of microemulsion of some insecticides and evaluating their efficacy against cotton leaf worm on cotton crop under laboratory and field conditions," *Entomol. Res.*, vol. 54, no. 5, p. e12733, May 2024, doi: https://doi.org/10.1111/1748-5967.12733.

[2] S. M. DeSalvio *et al.*, "A novel and efficient method for identifying cotton leafroll dwarf virus infection in upland cotton (Gossypium hirsutum)," *Plant Breed.*, vol. 142, no. 2, pp. 238–246, Apr. 2023, doi: https://doi.org/10.1111/pbr.13081.

[3] X. Feng *et al.*, "Deletion of GhSCY2D Causes Impaired Chloroplast Development and Temperature-Dependent Leaf Yellowing in Cotton (Gossypium hirsutum L.)," *Plant. Cell Environ.*, vol. 48, no. 7, pp. 4902–4917, Jul. 2025, doi: https://doi.org/10.1111/pce.15476.

[4] M. E. A. Whitehouse, C. R. Tann, and M. V Braunack, "Is 'pupae busting' or destroying overwintering pupae of Helicoverpa spp. (Lepidoptera: Noctuidae) still relevant today in Australian Bt cotton?," *Austral Entomol.*, vol. 62, no. 4, pp. 392–409, Nov. 2023, doi: https://doi.org/10.1111/aen.12669.

[5] G. Nachimuthu *et al.*, "Soil property differences and irrigated-cotton lint yield—Cause and effect? An on-farm case study across three cotton-growing regions in Australia," *Soil Use Manag.*, vol. 40, no. 2, p. e13065, Apr. 2024, doi: https://doi.org/10.1111/sum.13065.

[6] X. Li *et al.*, "High plant density optimizes leaf stomatal traits for accelerating the stomatal response rate at the lower cotton canopy," *Crop Sci.*, vol. 65, no. 1, p. e21443, Jan. 2025, doi: https://doi.org/10.1002/csc2.21443.

[7] X. Zhang *et al.*, "Wall-associated kinase GhWAK13 mediates arbuscular mycorrhizal symbiosis and Verticillium wilt resistance in cotton," *New Phytol.*, vol. 242, no. 5, pp. 2180–2194, Jun. 2024, doi: https://doi.org/10.1111/nph.19468.

[8] L. Li, F. Li, A. Liu, and X. Wang, "The prediction model of nitrogen nutrition in cotton canopy leaves based on hyperspectral visible-near infrared band feature fusion," *Biotechnol. J.*, vol. 18, no. 8, p. 2200623, Aug. 2023, doi: https://doi.org/10.1002/biot.202200623.

[9] R. Dhanalakshmi, K. Balakrishnan, S. Bam Bahadur, and R. and Gopalakrishnan, "Tomato leaf disease identification by modified inception based sequential convolution neural networks," *Imaging Sci. J.*, vol. 71, no. 5, pp. 408–424, Jul. 2023, doi: 10.1080/13682199.2023.2183318.

[10] V. Viswanathan and K. and Murugasamy, "Modified ensemble machine learning-based plant leaf disease detection model with optimized K-Means clustering," *Netw. Comput. Neural Syst.*, pp. 1–45, doi: 10.1080/0954898X.2024.2435492.

[11] R. T. Thivya Lakshmi, K. Jeevaa, and P. and Visu, "CoDet: A novel deep learning pipeline

for cotton plant detection and disease identification," *Automatika*, vol. 65, no. 2, pp. 662–674, Apr. 2024, doi: 10.1080/00051144.2024.2317093.

[12] A. K. Chaurasia, R. K. Singh, and A. Kumar, "Synthesis, optimization, characterization, anti-oxidant and anti-cancerous activity analysis of nanoparticles IA-AuNPs synthesized using leaf extract of soil grown Ipomoea aquatica," *J. Mol. Struct.*, vol. 1327, p. 141212, 2025, doi: 10.1016/j.molstruc.2024.141212.

[13] S. Swaraj and S. Aparna, "Water Wheel Plant Dingo Optimizer enabled Deep Convolutional Neural Network for disease detection using hyperspectral leaf image," *Infrared Phys. Technol.*, vol. 142, p. 105522, 2024, doi: https://doi.org/10.1016/j.infrared.2024.105522.

[14] J. Kotwal, R. Kashyap, P. M. Shafi, and V. Kimbahune, "Enhanced leaf disease detection: UNet for segmentation and optimized EfficientNet for disease classification," *Softw. Impacts*, vol. 22, p. 100701, 2024, doi: https://doi.org/10.1016/j.simpa.2024.100701.

[15] V. M. Amador-Luna, M. Herrero, M. Jiménez de la Parra, Á. G. Arribas, E. Ibáñez, and L. Montero, "Maximizing the neuroprotection from Citrus aurantium leaves: Optimization of a blended extract from a sequential extraction process with compressed fluids and NADES," *Adv. Sample Prep.*, vol. 13, p. 100149, 2025, doi: https://doi.org/10.1016/j.sampre.2025.100149.

[16] S. Nalini *et al.*, "Paddy Leaf Disease Detection Using an Optimized Deep Neural Network," *Comput. Mater. Contin.*, vol. 68, no. 1, pp. 1117–1128, 2021, doi: https://doi.org/10.32604/cmc.2021.012431.

[17] M. M. Islam *et al.*, "A deep learning model for cotton disease prediction using fine-tuning with smart web application in agriculture," *Intell. Syst. with Appl.*, vol. 20, no. January, p. 200278, 2023, doi: 10.1016/j.iswa.2023.200278.

[18] R. Rashid, W. Aslam, R. Aziz, and G. Aldehim, "A Modified MobileNetv3 Coupled With Inverted Residual and Channel Attention Mechanisms for Detection of Tomato Leaf Diseases," *IEEE Access*, vol. 13, pp. 52683–52696, 2025, doi: 10.1109/ACCESS.2025.3550205.

[19] Z. Chen, J. Feng, K. Zhu, Z. Yang, Y. Wang, and M. Ren, "YOLOv8-ACCW: Lightweight Grape Leaf Disease Detection Method Based on Improved YOLOv8," *IEEE Access*, vol. 12, pp. 123595–123608, 2024, doi: 10.1109/ACCESS.2024.3453379.

[20] S. M. N. Nobel *et al.*, "Palm Leaf Health Management: A Hybrid Approach for Automated Disease Detection and Therapy Enhancement," *IEEE Access*, vol. 12, pp. 9097–9111, 2024, doi: 10.1109/ACCESS.2024.3351912.

[21] M. Fahim-Ul-Islam, A. Chakrabarty, S. T. Ahmed, R. Rahman, H. H. Kwon, and M. J. Piran, "A Comprehensive Approach Toward Wheat Leaf Disease Identification Leveraging Transformer Models and Federated Learning," *IEEE Access*, vol. 12, pp. 109128–109156, 2024, doi: 10.1109/ACCESS.2024.3438544.

[22] M. E. Rayed, J. R. Jim, M. J. Islam, M. F. Mridha, M. M. Kabir, and M. J. Hossen, "MangoLeafXNet: An Explainable Deep Learning Model for Accurate Mango Leaf Disease Classification," *IEEE Access*, vol. 13, pp. 93977–94008, 2025, doi: 10.1109/ACCESS.2025.3571450.

[23] R. Maurya, L. Rajput, and S. Mahapatra, "RAI-Net: Tomato Plant Disease Classification Using Residual-Attention-Inception Network," *IEEE Access*, vol. 13, pp. 64832–64840, 2025, doi: 10.1109/ACCESS.2025.3559804.

[24] A. K. Sangaiah, F.-N. Yu, Y.-B. Lin, W.-C. Shen, and A. Sharma, "UAV T-YOLO-Rice: An Enhanced Tiny Yolo Networks for Rice Leaves Diseases Detection in Paddy Agronomy," *IEEE Trans. Netw. Sci. Eng.*, vol. 11, no. 6, pp. 5201–5216, 2024, doi: 10.1109/TNSE.2024.3350640.

[25] P. Khaparde *et al.*, "Experimental Investigation of Leaf Wetness Sensing Properties of MoS2 Nanoflowers-Based Flexible Leaf Wetness Sensor," *IEEE Sensors Lett.*, vol. 7, no. 2, pp. 1–4, 2023, doi: 10.1109/LSENS.2022.3229145.

[26] P. Khaparde, K. S. Patle, H. Borkar, J. Gangwar, A. K. Roy, and V. S. Palaparthy, "Investigating an Impact of Leaf Bending Radius and Angle for Flexible Leaf Wetness Sensor," *IEEE Sensors Lett.*, vol. 8, no. 3, pp. 1–4, 2024, doi: 10.1109/LSENS.2024.3355371.

[27] S. Abinaya, K. U. Kumar, and A. S. Alphonse, "Cascading Autoencoder With Attention Residual U-Net for Multi-Class Plant Leaf Disease Segmentation and Classification," *IEEE Access*, vol. 11, pp. 98153–98170, 2023, doi: 10.1109/ACCESS.2023.3312718.

[28] J. Chaki and D. Ghosh, "Deep Learning in Leaf Disease Detection (2014–2024): A Visualization-Based Bibliometric Analysis," *IEEE Access*, vol. 12, pp. 95291–95308, 2024, doi: 10.1109/ACCESS.2024.3425897.

[29] M. Masood *et al.*, "MaizeNet: A Deep Learning Approach for Effective Recognition of Maize Plant Leaf Diseases," *IEEE Access*, vol. 11, pp. 52862–52876, 2023, doi: 10.1109/ACCESS.2023.3280260.

[30] J. Ramkumar and R. Vadivel, "Multi-Adaptive Routing Protocol for Internet of Things based Ad-hoc Networks," *Wirel. Pers. Commun.*, vol. 120, no. 2, pp. 887–909, Apr. 2021, doi: 10.1007/s11277-021-08495-z.

[31] R. Jaganathan, S. Mehta, and R. Krishan, *Bio-Inspired intelligence for smart decision-making*, vol. i. 2024. doi: 10.4018/9798369352762.

[32] J. Ramkumar, K. S. Jeen Marseline, and D. R. Medhunhashini, "Relentless Firefly Optimization-Based Routing Protocol (RFORP) for Securing Fintech Data in IoT-Based Ad-Hoc Networks," *Int. J. Comput. Networks Appl.*, vol. 10, no. 4, pp. 668–687, 2023, doi: 10.22247/ijcna/2023/223319.

[33] M. Lingaraj, T. N. Sugumar, C. S. Felix, and J. Ramkumar, "Query aware routing protocol for mobility enabled wireless sensor network," *Int. J. Comput. Networks Appl.*, vol. 8, no. 3, pp. 258–267, 2021, doi: 10.22247/ijcna/2021/209192.

[34] J. Ramkumar, C. Kumuthini, B. Narasimhan, and S. Boopalan, "Energy Consumption Minimization in Cognitive Radio Mobile Ad-Hoc Networks using Enriched Ad-hoc On-demand Distance Vector Protocol," *2022 Int. Conf. Adv. Comput. Technol. Appl. ICACTA 2022*, pp. 1–6, Mar. 2022, doi: 10.1109/ICACTA54488.2022.9752899.

[35] A. Senthilkumar, J. Ramkumar, M. Lingaraj, D. Jayaraj, and B. Sureshkumar, "Minimizing Energy Consumption in Vehicular Sensor Networks Using Relentless Particle Swarm Optimization Routing," *Int. J. Comput. Networks Appl.*, vol. 10, no. 2, pp. 217–230, 2023, doi: 10.22247/ijcna/2023/220737.

[36] L. Mani, S. Arumugam, and R. Jaganathan, "Performance Enhancement of Wireless Sensor Network Using Feisty Particle Swarm Optimization Protocol," *ACM Int. Conf. Proceeding Ser.*, pp. 1–5, Dec. 2022, doi: 10.1145/3590837.3590907.

[37] J. Ramkumar and R. Vadivel, "Whale optimization routing protocol for minimizing energy consumption in cognitive radio wireless sensor network," *Int. J. Comput. Networks Appl.*, vol. 8, no. 4, pp. 455–464, 2021, doi: 10.22247/ijcna/2021/209711.

[38] J. Ramkumar, R. Karthikeyan, and M. Lingaraj, "Optimizing IoT-Based Quantum Wireless Sensor Networks Using NM-TEEN Fusion of Energy Efficiency and Systematic Governance," in *Lecture Notes in Electrical Engineering*, V. Shrivastava, J. C. Bansal, and B. K. Panigrahi, Eds., Springer Science and Business Media Deutschland GmbH, 2025, pp. 141–153. doi: 10.1007/978-981-97-6710-6_12.

[39] J. Ramkumar, R. Karthikeyan, and V. Valarmathi, "Alpine Swift Routing Protocol (ASRP) for Strategic Adaptive Connectivity Enhancement and Boosted Quality of Service in Drone Ad Hoc Network (DANET)," *Int. J. Comput. Networks Appl.*, vol. 11, no. 5, pp. 726–748, 2024, doi: 10.22247/ijcna/2024/45.

[40] S. P. Geetha, N. M. S. Sundari, J. Ramkumar, and R. Karthikeyan, "Energy Efficient Routing In Quantum Flying Ad Hoc Network (Q-FANET) Using Mamdani Fuzzy Inference Enhanced Dijkstra's Algorithm (MFI-EDA)," *J. Theor. Appl. Inf. Technol.*, vol. 102, no. 9, pp. 3708–3724, 2024, [Online]. Available: https://www.scopus.com/inward/record.uri?eid=2-s2.0-85197297302&partnerID=40&md5=72d51668bee6239f09a59d2694df67d6

[41] R. Vadivel and J. Ramkumar, "QoS-enabled improved cuckoo search-inspired protocol (ICSIP) for IoT-based healthcare applications," in *Incorporating the Internet of Things in Healthcare Applications and Wearable Devices*, IGI Global, 2019, pp. 109–121. doi: 10.4018/978-1-7998-1090-2.ch006.

[42] J. Ramkumar and R. Vadivel, "Improved Wolf prey inspired protocol for routing in cognitive radio Ad Hoc networks," *Int. J. Comput. Networks Appl.*, vol. 7, no. 5, pp. 126–136, 2020, doi: 10.22247/ijcna/2020/202977.

[43] D. Jayaraj, J. Ramkumar, M. Lingaraj, and B. Sureshkumar, "AFSORP: Adaptive Fish Swarm Optimization-Based Routing Protocol for Mobility Enabled Wireless Sensor Network," *Int. J. Comput. Networks Appl.*, vol. 10, no. 1, pp. 119–129, 2023, doi: 10.22247/ijcna/2023/218516.

[44] P. Menakadevi and J. Ramkumar, "Robust Optimization Based Extreme Learning Machine for Sentiment Analysis in Big Data," in *2022 International Conference on Advanced*

Computing Technologies and Applications, ICACTA 2022, Institute of Electrical and Electronics Engineers Inc., 2022. doi: 10.1109/ICACTA54488.2022.9753203.

[45] M. P. Swapna, J. Ramkumar, and R. Karthikeyan, "Energy-Aware Reliable Routing with Blockchain Security for Heterogeneous Wireless Sensor Networks," in *Lecture Notes in Networks and Systems*, V. Goar, M. Kuri, R. Kumar, and T. Senjyu, Eds., Springer Science and Business Media Deutschland GmbH, 2025, pp. 713–723. doi: 10.1007/978-981-97-6106-7_43.

[46] R. Jaganathan and V. Ramasamy, "Performance modeling of bio-inspired routing protocols in Cognitive Radio Ad Hoc Network to reduce end-to-end delay," *Int. J. Intell. Eng. Syst.*, vol. 12, no. 1, pp. 221–231, 2019, doi: 10.22266/IJIES2019.0228.22.

[47] R. Jaganathan, S. Mehta, and R. Krishan, *Intelligent Decision Making Through Bio-Inspired Optimization*. IGI Global, 2024. doi: 10.4018/979-8-3693-2073-0.

[48] J. Ramkumar, S. S. Dinakaran, M. Lingaraj, S. Boopalan, and B. Narasimhan, "IoT-Based Kalman Filtering and Particle Swarm Optimization for Detecting Skin Lesion," in *Lecture Notes in Electrical Engineering*, K. Murari, S. Kamalasadan, and N. P. Padhy, Eds., Springer Science and Business Media Deutschland GmbH, 2023, pp. 17–27. doi: 10.1007/978-981-19-8353-5_2.

[49] J. Ramkumar and R. Vadivel, "Improved frog leap inspired protocol (IFLIP) – for routing in cognitive radio ad hoc networks (CRAHN)," *World J. Eng.*, vol. 15, no. 2, pp. 306–311, 2018, doi: 10.1108/WJE-08-2017-0260.

[50] J. Ramkumar, A. Senthilkumar, M. Lingaraj, R. Karthikeyan, and L. Santhi, "Optimal Approach for Minimizing Delays in IoT-Based Quantum Wireless Sensor Networks Using NM-Leach Routing Protocol," *J. Theor. Appl. Inf. Technol.*, vol. 102, no. 3, pp. 1099–1111, 2024, [Online]. Available: https://www.scopus.com/inward/record.uri?eid=2-s2.0-85185481011&partnerID=40&md5=bf0ff974ceabc0ad58e589b28797c684

[51] K. S. J. Marseline, J. Ramkumar, and D. R. Medhunhashini, "Sophisticated Kalman Filtering-Based Neural Network for Analyzing Sentiments in Online Courses," in *Smart Innovation, Systems and Technologies*, A. K. Somani, A. Mundra, R. K. Gupta, S. Bhattacharya, and A. P. Mazumdar, Eds., Springer Science and Business Media Deutschland GmbH, 2024, pp. 345–358. doi: 10.1007/978-981-97-3690-4_26.

[52] R. Jaganathan and R. Vadivel, "Intelligent Fish Swarm Inspired Protocol (IFSIP) for Dynamic Ideal Routing in Cognitive Radio Ad-Hoc Networks," *Int. J. Comput. Digit. Syst.*, vol. 10, no. 1, pp. 1063–1074, 2021, doi: 10.12785/ijcds/100196.

[53] J. Ramkumar and R. Vadivel, "CSIP—cuckoo search inspired protocol for routing in cognitive radio ad hoc networks," in *Advances in Intelligent Systems and Computing*, Springer Verlag, 2017, pp. 145–153. doi: 10.1007/978-981-10-3874-7_14.

[54] B. Suchitra, J. Ramkumar, and R. Karthikeyan, "Frog Leap Inspired Optimization-Based Extreme Learning Machine for Accurate Classification of Latent Autoimmune Diabetes in Adults (LADA)," *J. Theor. Appl. Inf. Technol.*, vol. 103, no. 2, pp. 472–494, 2025, [Online]. Available: https://www.scopus.com/inward/record.uri?eid=2-s2.0-85217140979&partnerID=40&md5=9540433c16d5ff0f6c2de4b8c43a4812

[55] J. Ramkumar, B. Varun, V. Valarmathi, D. R. Medhunhashini, and R. Karthikeyan, "Jaguar-Based Routing Protocol (JRP) For Improved Reliability and Reduced Packet Loss in Drone Ad-Hoc Networks (DANET)," *J. Theor. Appl. Inf. Technol.*, vol. 103, no. 2, pp. 696–713, 2025, [Online]. Available: https://www.scopus.com/inward/record.uri?eid=2-s2.0-85217213044&partnerID=40&md5=e38a375e46cf43c95d6702a3585a7073

[56] J. Ramkumar, V. Valarmathi, and R. Karthikeyan, "Optimizing Quality of Service and Energy Efficiency in Hazardous Drone Ad-Hoc Networks (DANET) Using Kingfisher Routing Protocol (KRP)," *Int. J. Eng. Trends Technol.*, vol. 73, no. 1, pp. 410–430, 2025, doi: 10.14445/22315381/IJETT-V73I1P135.

[57] R. Jaganathan, K. Rajendran, and P. S. Ponnukumar, "Peregrine Falcon Optimization Routing Protocol (PFORP) for Achieving Ultra-Low Latency and Boosted Efficiency in 6G Drone Ad-Hoc Networks (DANET)," *Int. J. Comput. Digit. Syst.*, vol. 17, no. 1, pp. 1–18, 2025, doi: 10.12785/ijcds/1571111848.

[58] R. Jaganathan, S. Mehta, and R. Krishan, "Preface," *Intell. Decis. Mak. Through Bio-Inspired Optim.*, pp. xiii–xvi, 2024, [Online]. Available:

https://www.scopus.com/inward/record.uri?eid=2-s2.0-85192858710&partnerID=40&md5=f8f1079e8772bd424d2cdd979e5f2710

[59] R. Jaganathan, S. Mehta, and R. Krishan, "Preface," *Bio-Inspired Intell. Smart Decis.*, pp. xix–xx, 2024, [Online]. Available: https://www.scopus.com/inward/record.uri?eid=2-s2.0-85195725049&partnerID=40&md5=7a2aa7adc005662eebc12ef82e3bd19f

[60] J. Ramkumar and D. Ravindran, "Machine learning and robotics in urban traffic flow optimization with graph neural networks and reinforcement learning," in *Machine Learning and Robotics in Urban Planning and Management*, 2025, pp. 83–104. doi: 10.4018/979-8-3693-9410-6.ch005.